ORIGINAL PAPER

R. Le Bayon · C. de Capitani · M. Frey

Modelling phase–assemblage diagrams for magnesian metapelites in the system K_2O–FeO–MgO–Al_2O_3–SiO_2–H_2O: geodynamic consequences for the Monte Rosa nappe, Western Alps

Abstract Magnesian metamorphic rocks with metapelitic mineral assemblage and composition are of great interest in metamorphic petrology for their ability to constrain P–T conditions in terranes where metamorphism is not easily visible. Phase–assemblage diagrams for natural and model magnesian metapelites in the system KFMASH are presented to document how phase relationships respond to water activity, bulk composition, pressure and temperature. The phase assemblages displayed on these phase diagrams are consistent with natural mineral assemblages occurring in magnesian metapelites. It is shown that the equilibrium assemblages at high pressure conditions are very sensitive to a(H_2O). Specifically, the appearance of the characteristic HP assemblage chloritoid–talc–phengite–quartz (with excess H_2O) in the magnesian metapelites of the Monte Rosa nappe (Western Alps) is due to the reduction of a(H_2O). Furthermore, the mineral assemblages are determined by the whole-rock FeO/(FeO + MgO) ratio and effective Al content X_A as well as P and T. The predicted mineral associations for the low- and high-X_A model bulk compositions of magnesian metapelites at high pressure are not dependent on the X_A variations as they show a similar sequence of mineral assemblages. Above 20 kbar, the prograde sequence of assemblages associated with phengite (with excess SiO_2 and H_2O) for low- and high-X_A bulk compositions of magnesian metapelites is: carpholite–chlorite $\rightarrow$ chlorite–chloritoid $\rightarrow$ chloritoid–talc $\rightarrow$ chloritoid–talc–kyanite $\rightarrow$ talc–garnet–kyanite $\rightarrow$ garnet–kyanite $\pm$ biotite. At low to medium P–T conditions, a low-X_A stabilises the phengite-bearing assemblages associated with chlorite, chlorite + K-feldspar and chlorite + biotite while a high-X_A results in the chlorite–phengite bearing assemblages associated with pyrophyllite, andalusite, kyanite and carpholite. A high-X_A magnesian metapelite with nearly iron-free content stabilises the talc–kyanite–phengite assemblage at moderate to high P–T conditions. Taking into account the effective bulk composition and a(H_2O) involved in the metamorphic history, the phase–assemblage diagrams presented here may be applied to all magnesian metapelites that have compositions within the system KFMASH and therefore may contribute to gaining insights into the metamorphic evolution of terranes. As an example, the magnesian metapelites of the Monte Rosa nappe have been investigated, and an exhumation path with P–T conditions for the western roof of the Monte Rosa nappe has been derived for the first time. The exhumation shows first a near-isothermal decompression from the Alpine eclogite peak conditions around 24 kbar and 505°C down to approximately 8 kbar and 475°C followed by a second decompression with concomitant cooling.

R. Le Bayon (✉) · C. de Capitani · M. Frey
Department of Earth Sciences, University of Basel,
Bernoullistrasse 30, 4056 Basel, Switzerland
E-mail: rlebayon@geo.tu-darmstadt.de
Tel.: +49-61-51166541
Fax: +49-61-51164021

Present address: R. Le Bayon
Institut für Geowissenschaften, Technische Universität Darmstadt,
Schnittspahnstrasse 9, 64287 Darmstadt, Germany

Introduction

One of the aims of metamorphic petrology is to determine the pressure–temperature history of natural rocks, and thus to aid understanding of orogenic processes. In mountain belts consisting mostly of granitoid basement, it is very difficult to carry out metamorphic studies because the absence of fluid and deformation usually leads to sluggish reactions. In such terranes without other metamorphic rocks, the presence of very unusual and rather rare highly magnesian and Fe-poor rocks of metapelitic composition gives us a chance to understand their metamorphic history. Because of their

well-preserved high grade metapelitic mineral associations and their reactions (e.g. Chopin and Schreyer 1983), the magnesian metamorphic rocks of metapelitic composition have great potential for constraining equilibration conditions, reaction history and P–T evolution.

The principal goal of this study is to improve our understanding of the phase relationships in magnesian metamorphic rocks with metapelitic bulk compositions mostly comprised by the system K_2O–FeO–MgO–Al_2O_3–SiO_2–H_2O (KFMASH) as a function of pressure, temperature, water activity and bulk-rock composition, and thus to constrain and interpret large-scale geodynamic evolution. This paper presents phase–assemblage diagrams for magnesian metapelites in the system KFMASH based on currently available thermodynamic data and experimental calibrations. They serve as qualitative and quantitative tools for the interpretation of natural magnesian metapelites.

Calculated phase–assemblage diagrams for specific bulk compositions, based on the minimisation of the Gibbs free energy, provide a more complete and realistic view than conventional petrogenetic grids or P–T stability fields for single minerals even if they were a great help in the last decades (e.g. Schreyer and Seifert 1969; Schreyer 1988; Massonne and Schreyer 1989; Spear and Cheney 1989; El Shazly and Liou 1991; Vidal et al. 1992).

The aims of this paper are: (1) to provide an introduction to the petrology and mineral chemistry of magnesian metapelites using examples from the Monte Rosa nappe (Western Alps); (2) to describe the modelling methodology used in this study; (3) to present petrologic particularities of magnesian metapelites highlighted by phase–assemblage diagrams with $a(H_2O) = 1$; (4) to investigate the effect of water activity on the stability of mineral assemblages in magnesian metapelites by calculating phase–assemblage diagrams; (5) to present and discuss P–T phase–assemblage diagrams with $a(H_2O) = 0.6$ for model compositions of magnesian metapelites; (6) to investigate the changes in mineral assemblages caused by varying pressure, temperature, $FeO/(FeO + MgO)$ ratio and effective Al content; and (7) to compare the sequences of calculated mineral assemblages with those in well-studied natural magnesian metapelites occurring in the Western Alps (Gran Paradiso, Dora Maira and Monte Rosa nappes). These sequences are then used to derive P–T histories for the Monte Rosa nappe to gain insight into its subduction and exhumation history within the framework of general alpine geodynamic evolution.

Petrology and mineral chemistry of magnesian metapelites: examples from the Monte Rosa nappe

Magnesian metapelites are unusual and rather rare rocks. For bulk compositions mostly comprised by the system KFMASH, these metapelites have MgO- an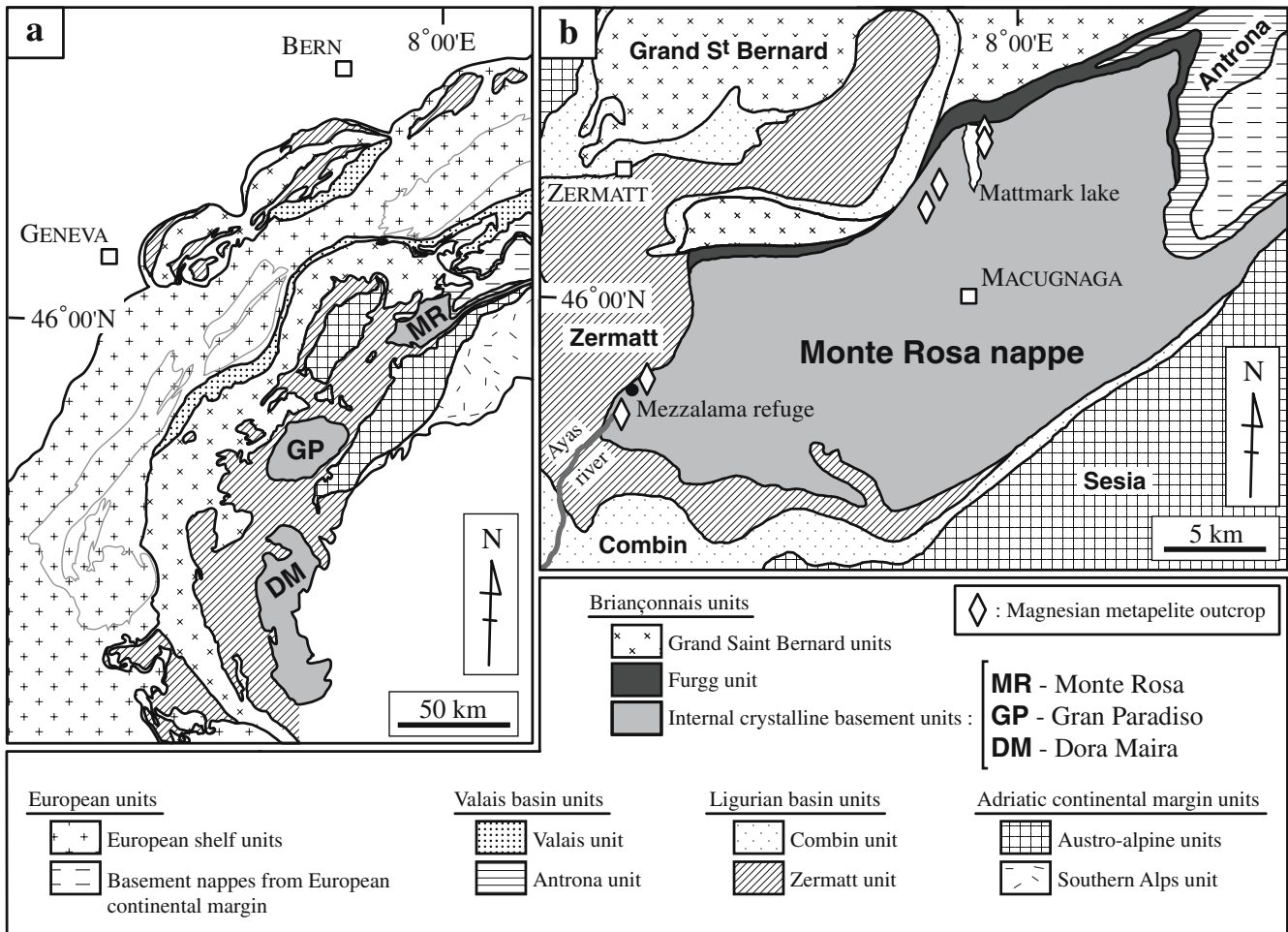d Al_2O_3-rich bulk compositions, various effective Al contents X_A ($X_A = (Al_2O_3\text{-}3K_2O)/(Al_2O_3\text{-}3K_2O + FeO + MgO)$), a $FeO/(FeO + MgO)$ ratio < 0.5 that can nearly reach 0.0 (Table 1). Common mineral assemblages such as Mg–chlorite + muscovite + quartz, talc + phengite + quartz, talc + chloritoid + quartz and pyrope + kyanite + coesite are recognised in magnesian metapelites from low and high metamorphic grade terranes (Chinner and Dixon 1973; Abraham and Schreyer 1976; Chopin 1981, 1983; Chopin et al. 1991; Sharp et al. 1993; Demény et al. 1997). In addition, specific Mg-rich, Fe-poor talc–kyanite schists first studied by Vrana and Barr (1972) were defined by Schreyer (1973, 1974, 1977) as whiteschists.

Over the past several decades, different origins have been suggested for the protolith of Alpine magnesian metapelites: Mg-rich evaporitic sediment (Chopin and Monié 1984), Mg-metasomatism of gneisses and micaschists by metamorphic fluids along shear zones (Sharp et al. 1993), and metasomatic transformations of granite along HP shear zones in the Monte Rosa (Bearth 1952; Dal Piaz 1971; Dal Piaz and Lombardo 1986). More recently, Pawlig and Baumgartner (2001) have argued for a pre-Alpine argillitic alteration leading to chlorite-rich metasomatic alteration of the Monte Rosa granite from stable isotope constrains on HP magnesian metapelites.

Magnesian metapelites from the Monte Rosa nappe

The Monte Rosa nappe is one of the three internal massifs in the Western Alps (Fig. 1). The Monte Rosa nappe consists mainly of Variscan granites intruded into the high grade metapelitic basement during the Permian (270 ± 4 Ma, Pawlig and Baumgartner 2001). The magnesian metapelites occur in shear zones or as bands in the Variscan granites. Magnesian metapelites are only recognised in the structural top of the Monte Rosa nappe. The structural and most westerly top of the Monte Rosa nappe was selected to help us understand the exhumation of eclogite facies rocks because it was not affected by the late-Alpine Barrovian Lepontine metamorphic phase (Todd and Engi 1997; Nagel et al. 2002).

Two distinct types of magnesian metapelite (Table 1) have been found in the Monte Rosa nappe. The first is a chloritoid-bearing rock with $0.35 > FeO/(FeO + MgO)$ ratio ≥ 0.1 and $0.17 \leq X_A \leq 0.35$ located in the upper part of Val d'Ayas (Italy) at the base of the Piccolo Ghiacciaio di Verra (Dal Piaz 1971; Dal Piaz and Lombardo 1986; Pawlig and Baumgartner 2001). Val d'Ayas magnesian metapelites occur as bands up to 1–2 m wide in undeformed granite above the Mezzalama refuge and above its underlying glacial lake in a shear zone up to 40 m wide. The core of this shear zone in the Monte Rosa granite is composed of magnesian metapelites up to 10–15 m wide. The second is a talc–kyanite bearing rock with a $FeO/(FeO + MgO)$ ratio < 0.1 and $0.37 \leq X_A \leq 0.46$ found in layers up to 0.5 m wide parallel to the foliation of the surrounding gneiss on the

Fig. 1 Simplified geological maps of the Western Alps (**a**) and the Monte Rosa nappe region (**b**), adapted from Spicher (1980) and Escher et al. (1993). Locations of magnesian metapelites studied in this paper, occurring in the upper part of the Val d'Ayas (Italy) and around the Mattmark lake (Switzerland) are reported on map (**b**). Val d'Ayas magnesian metapelites occur above the Mezzalama refuge and above its underlying glacial lake (2,750 m asl; swiss co-ordinates: 625.050/084.143). Magnesian metapelites occurring in the Mattmark lake area are located on the eastern (2,210 m asl; swiss co-ordinates: 640.700/099.575) and western (2,750 m asl; swiss co-ordinates: 639.375/096.875) sides of the lake

eastern and western shores of the Mattmark lake in the upper part of the Saas valley (Switzerland). These different magnesian metapelites of the Monte Rosa nappe show a series of critical assemblages (Fig. 2) including Cld–Tlc–Phe–Qtz, Ky–Chl–Phe–Qtz, Chl–Ms–Qtz and Tlc–Ky–Phe–Qtz (Mineral abbreviations after Kretz 1983; Phe = phengite). Microscopic observations reveal that several breakdown stages occur in the magnesian metapelites.

The first type of magnesian metapelite, with $0.35 > FeO/(FeO + MgO)$ ratio ≥ 0.1 and $0.17 \leq X_A \leq 0.35$, includes one specimen almost free of late metamorphic overprint. This rock displays a Cld–Tlc assemblage (Fig. 2a) where contacts between these two minerals are preserved. In this type of magnesian metapelites, chloritoid with $0.45 \leq X_{Mg} \leq 0.62$ and talc with $0.94 \leq X_{Mg} \leq 0.96$ (Table 2) are in many cases replaced (Fig. 2b–c) by a first generation of large chlorite crystals with $0.81 \leq X_{Mg} \leq 0.86$ and $5.30 \leq Si$ (p.f.u) ≤ 5.67 (Table 2). Sometimes, the large chlorite is

associated with tiny grains of kyanite in a foliation made of quartz and phengite with $6.50 \leq Si$ (p.f.u) ≤ 6.82 (Table 2). In a later reaction event, the remnants of chloritoid and talc but also kyanite and large chlorite broke down to an assemblage of small second generation chlorite crystals with $X_{Mg} \sim 0.97$ and $5.36 \leq Si$ (p.f.u) ≤ 5.42, associated with small flakes of muscovite (or low-Si phengite) with $6.0 \leq Si$ (p.f.u) ≤ 6.1 and with up to 20 mol% paragonite in solid solution (Fig. 2d, Table 2).

The second kind of magnesian metapelite that is nearly iron-free with a $FeO/(FeO + MgO)$ ratio < 0.1, contains a Tlc–Ky assemblage where talc with $X_{Mg} \sim 0.99$ (Table 2) is only preserved as inclusions in kyanite (Fig. 2e). Kyanite is associated with a first generation of large chlorites with $0.96 \leq X_{Mg} \leq 0.98$ and $5.49 \leq Si$ (p.f.u) ≤ 5.52 (Table 2), large phengite crystals and quartz in the rock foliation. The Si content of the apparently first generation of phengite ranges between 6.20 and 6.85 p.f.u (Table 2). In the quartz-phengitic

Table 1 Bulk compositions of samples of different natural magnesian metapelites divided into a low and a high effective Al content X_A type ($X_A = (Al_2O_3-3K_2O)/(Al_2O_3-3K_2O+FeO+MgO)$)

	High-X_A sample											Low-X_A sample					
Reference	99MR103	99MR02	99MR04	99MR37	SK1-00	7-20b	6-298a	7-37	MZ	17341	17691	99MR09	99MR103b	99MR104	99MR105	99MR107	99MR108
	(1)	(1)	(1)	(1)	(1)	(2)	(2)	(3)	(4)	(5)	(5)	(1)	(1)	(1)	(1)	(1)	(1)
Location	MR	MR	MR	MR	DM	GP	GP	GP	FU	DM	DM	MR	MR	MR	MR	MR	MR
SiO$_2$ wt.%	63.41	74.13	71.27	70.64	69.62	32.49	33.77	43.71	65.99	69.70	74.40	68.68	69.58	69.68	68.14	70.24	70.29
TiO$_2$	0.51	0.24	0.24	0.31	0.46	0.19	0.08	0.34	0.34	0.34	0.29	0.30	0.41	0.44	0.40	0.38	0.46
Al$_2$O$_3$	16.70	13.51	13.86	14.15	16.43	26.58	28.65	24.17	17.95	17.92	14.26	15.09	14.89	14.54	16.30	14.67	15.26
FeO	0.00	0.00	0.00	0.00	0.00	9.57	8.63	3.22	2.46	0.32	0.41	0.00	0.00	0.00	0.00	0.00	0.00
Fe$_2$O$_3$	3.95	0.31	0.53	0.69	0.39	2.86	3.33	4.28	0.00	0.00	0.00	0.87	2.57	1.74	1.33	1.46	0.98
MnO	0.04	0.00	0.00	0.00	0.01	0.14	0.14	0.06	0.00	0.01	0.01	0.00	0.02	0.00	0.02	0.02	0.02
MgO	7.01	5.29	4.80	5.27	7.25	15.69	13.53	14.67	5.84	7.47	6.08	4.87	4.65	5.02	4.26	4.56	3.97
CaO	0.40	0.18	0.14	0.21	0.17	0.73	0.58	0.21	0.00	0.14	0.03	0.18	0.32	0.32	0.31	0.30	0.33
Na$_2$O	0.21	0.00	0.32	0.30	0.23	0.14	0.12	0.16	0.27	0.19	0.21	0.34	0.00	0.30	0.47	0.42	0.38
K$_2$O	3.70	2.92	3.49	3.54	3.46	3.08	3.08	2.64	4.04	2.73	3.04	4.57	4.17	4.19	5.05	4.36	4.72
P$_2$O$_5$	0.34	0.14	0.15	0.15	0.06	0.40	0.50	0.29	0.00	0.07	0.04	0.14	0.27	0.28	0.26	0.27	0.27
H$_2$O	3.73	3.28	5.20	4.74	1.92	8.48	7.76	6.06	3.78	1.48	1.56	4.96	3.12	3.49	3.46	3.32	3.32
Total	100.00	100.00	100.00	100.00	100.00	100.35	100.17	99.81	100.33	100.37	100.33	100.00	100.00	100.00	100.00	100.00	100.00
A = Al$_2$O$_3$-3K$_2$O%	34.64	46.03	39.11	37.47	44.32	38.39	43.55	42.77	41.26	55.54	44.20	21.30	18.48	17.41	23.03	25.47	19.62
F = FeO%	21.99	2.70	5.50	6.59	2.57	26.88	26.09	18.61	17.41	1.83	3.53	17.60	14.82	18.11	18.30	24.75	11.13
M = MgO%	43.37	51.26	55.38	55.94	53.11	34.73	30.36	38.61	41.33	42.64	52.28	61.09	66.70	64.48	58.67	49.77	69.25
FeO/(FeO+MgO)	0.336	0.050	0.090	0.105	0.046	0.436	0.462	0.325	0.296	0.041	0.063	0.224	0.182	0.219	0.238	0.332	0.138

The location of the samples are *MR* Monte Rosa, *FU* Furgg unit, *GP* Gran Paradiso, and *DM* Dora Maira. The source of the data is *(1)* this study, *(2)* Chopin (1984), *(3)* Chopin (1979), *(4)* Chopin and Monié (1984), *(5)* Tilton et al. (1991)

foliation, kyanite porphyroclasts and phengite were later replaced by an assemblage consisting of small second generation chlorite with $X_{Mg} \sim 0.98$ and $5.42 \leq Si$ (p.f.u) ≤ 5.46 and muscovite with $6.0 \leq Si$ (p.f.u) ≤ 6.15 (Fig. 2e, Table 2).
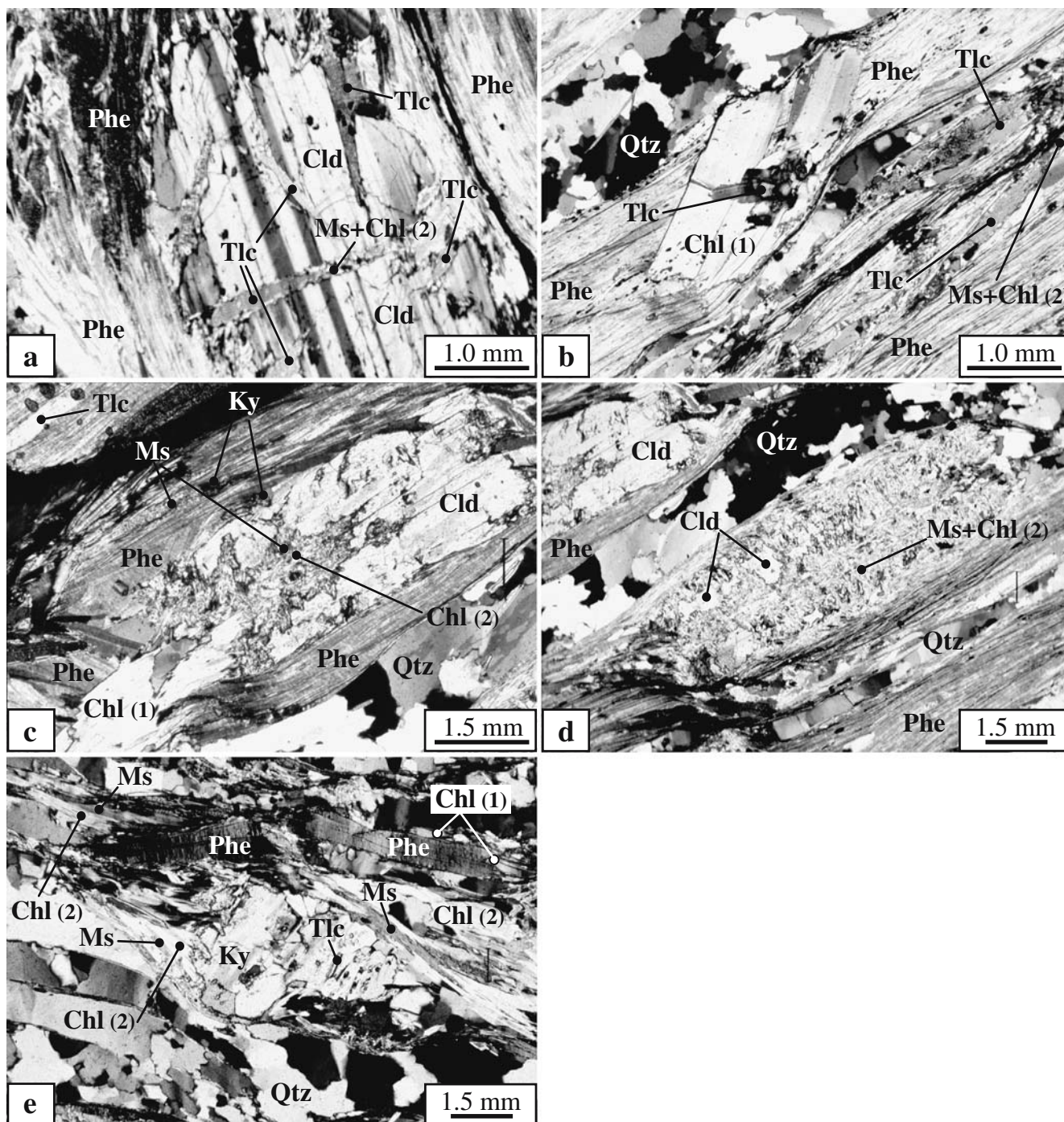
Methodology

General approach

We will illustrate the relationship between the P and T of equilibration and observed mineral assemblage, and examine the influence of water activity and bulk composition on the coexisting assemblages in a particular magnesian metapelite. We approach this problem by calculating phase–assemblage diagrams for different average, idealised and representative magnesian metapelite bulk compositions, which are expected to develop the common assemblages. The comparison of the results of the calculations with the natural samples will test and validate the modelling.

Phase–assemblage diagrams

Our thermodynamic analyses are based on phase–assemblage diagrams calculated with the thermodynamic software DOMINO (de Capitani and Brown 1987; de Capitani 1994; Biino and de Capitani 1995). This approach uses a minimisation of the total Gibbs free energy to predict the equilibrium assemblages for different pressures, temperatures and bulk compositions. Three types of phase–assemblage diagrams are used to present the results of this study. The first has P and T as coordinates. It is a phase–assemblage diagram showing different mineralogical phases in equilibrium assemblages for various pressure and temperature conditions. The second is phase–assemblage diagram with pressure or temperature as a function of water activity. The third is a phase–assemblage diagram, where pressure or temperature is a function of the chemical composition, such as the FeO/(FeO + MgO) ratio, and the effective Al content X_A.

Thermodynamic database

We used the updated thermodynamic database JUNE.92 of Berman (1988). The standard state enthalpy of formation from the elements ($\Delta_f H°$) and entropy (S°) values of Fe- and Mg-chloritoid, carpholite (Car) and daphnite (Dap) (Table 3) were retrieved by mathematical optimisation with the program MINOS by Murtagh and Saunders (1987) from published experiments or approximate P–T location of reactions. For Fe- and Mg-chloritoid, we used the experimental brackets of Ganguly (1969) and Vidal et al. (1994) for the reactions $3Fe\text{-}Cld \Leftrightarrow Grt + 4Dsp + H_2O$ and $3Fe\text{-}Cld \Leftrightarrow$

Fig. 2 Photomicrographs (polarised light) showing some petrological relationships in the magnesian metapelites from the Monte Rosa nappe. **a** Crystal of chloritoid with inclusions of talc, coexisting with talc, phengite, quartz (sample 99MR107, Val d'Ayas area). **b** Talc crystals aligned in the quartz–phengitic foliation. Talc has partially broken down to large first generation chlorite [Chl (1)] and deformed assemblage of small second generation chlorite [Chl (2)] and muscovite (sample 99MR107, Val d'Ayas area). **c** Chloritoid crystal in a foliation made up of talc, phengite and quartz partially replaced by large first generation chlorite [Chl (1)] and tiny kyanite grains and later by a late undeformed assemblage consisting of small muscovite and small second generation chlorite [Chl (2)]. Note the breakdown of kyanite associated with phengite to an assemblage of tiny muscovite grains (sample 99MR107, Val d'Ayas area). **d** In the centre of the photograph, some remnants of chloritoid demonstrate a nearly complete replacement by an equilibrated undeformed assemblage of fine-grained second generation chlorite [Chl (2)] and small muscovite (sample 99MR107, Val d'Ayas area). **e** Porphyroclast of kyanite containing inclusions of talc coexisting with phengite and quartz. This paragenesis is partially replaced by a deformed assemblage of small second generation chlorite [Chl (2)] and small muscovite (sample 99MR56, Mattmark lake area)

Table 2 Representative microprobe mineral analyses in magnesian metapelites of the Monte Rosa nappe. 99MR107 (sample with low-X_A content and FeO/(FeO+MgO) ratio ≥ 0.1) from Val d'Ayas area; 99MR03 (sample with high-X_A content and FeO/(FeO+MgO) ratio < 0.1) from Mattmark lake area. The chloritoid, talc, phengite and chlorite formulae are calculated on 12, 22, 22 and 28 anhydrous oxygen basis, respectively

Sample	99MR107														99MR03							
	Cld	Cld	Tlc	Tlc	Phe	Phe	Phe	Chl (1)	Chl (1)	Chl (1)	Ms	Ms	Chl (2)	Chl (2)	Tlc	Phe	Phe	Phe	Phe	Chl (1)	Ms	Chl (2)
SiO_2	25.76	25.67	62.01	61.78	50.88	50.85	47.48	28.83	28.35	27.57	46.69	45.79	28.72	27.89	61.96	50.61	50.33	48.27	46.69	28.75	45.66	28.51
TiO_2	0.00	0.00	0.13	0.00	0.05	0.05	0.21	0.10	0.00	0.10	0.03	0.24	0.00	0.00	0.03	0.16	0.16	0.21	0.24	0.27	0.37	0.16
Al_2O_3	43.32	42.55	0.45	0.21	26.96	27.76	28.25	21.31	21.58	21.92	37.46	36.73	24.47	24.39	0.34	26.74	27.81	31.70	34.61	23.20	36.00	24.11
FeO	13.40	15.4	2.98	2.48	0.99	1.01	1.30	9.03	10.42	9.44	0.11	0.17	1.80	1.78	0.70	0.36	0.17	0.11	0.13	1.22	0.09	1.28
MnO	0.27	0.15	0.00	0.00	0.10	0.08	0.08	0.00	0.09	0.05	0.00	0.00	0.00	0.00	0.00	0.01	0.00	0.00	0.02	0.00	0.00	0.04
MgO	9.61	8.51	29.96	30.05	4.15	4.45	4.56	26.47	25.78	26.36	1.00	1.19	30.84	30.23	31.04	4.06	3.69	2.44	1.30	30.86	0.83	30.39
CaO	0.00	0.00	0.00	0.00	0.00	0.01	0.00	0.00	0.01	0.00	0.00	0.06	0.01	0.00	0.00	0.00	0.00	0.00	0.08	0.03	0.03	0.00
Na_2O	0.00	0.00	0.00	0.00	0.30	0.24	0.37	0.00	0.00	0.00	0.53	1.51	0.00	0.00	0.00	0.26	0.38	0.70	0.98	0.01	1.30	0.02
K_2O	0.00	0.00	0.00	0.00	11.50	11.09	10.76	0.02	0.03	0.00	10.55	9.14	0.04	0.03	0.03	11.13	11.13	10.73	10.32	0.01	9.96	0.02
Total	92.36	92.28	95.53	94.52	94.93	95.54	93.02	85.76	86.27	85.46	96.37	94.82	85.88	84.32	94.07	93.33	93.68	94.17	94.38	84.35	94.26	84.50
Si	2.009	2.023	7.924	7.957	6.816	6.751	6.513	5.665	5.586	5.464	6.097	6.063	5.425	5.368	7.953	6.854	6.786	6.470	6.240	5.513	6.108	5.457
Ti	0.000	0.000	0.012	0.000	0.005	0.005	0.022	0.015	0.000	0.015	0.003	0.024	0.000	0.000	0.000	0.016	0.016	0.021	0.024	0.039	0.037	0.023
Al	3.982	3.952	0.068	0.032	4.256	4.343	4.567	4.934	5.011	5.120	5.765	5.732	5.448	5.533	0.051	4.268	4.419	5.007	5.451	5.243	5.675	5.438
Fe	0.874	1.015	0.318	0.267	0.111	0.112	0.149	1.484	1.717	1.564	0.012	0.019	0.284	0.286	0.075	0.041	0.019	0.012	0.015	0.196	0.010	0.205
Mn	0.018	0.010	0.000	0.000	0.011	0.009	0.009	0.000	0.015	0.008	0.000	0.000	0.000	0.000	0.000	0.001	0.000	0.000	0.002	0.000	0.000	0.006
Mg	1.117	1.000	5.707	5.770	0.829	0.881	0.932	7.754	7.573	7.789	0.195	0.235	8.685	8.675	5.940	0.820	0.742	0.488	0.259	8.822	0.166	8.672
Ca	0.000	0.000	0.000	0.000	0.000	0.001	0.000	0.000	0.002	0.000	0.000	0.009	0.002	0.000	0.000	0.000	0.000	0.000	0.011	0.006	0.004	0.000
Na	0.000	0.000	0.000	0.000	0.078	0.062	0.098	0.000	0.002	0.000	0.134	0.388	0.002	0.000	0.000	0.068	0.099	0.182	0.254	0.006	0.337	0.000
K	0.000	0.000	0.000	0.000	1.965	1.878	1.883	0.003	0.004	0.000	1.757	1.544	0.005	0.004	0.005	1.923	1.914	1.834	1.759	0.001	1.699	0.000
$\sum$ cat.	8.000	8.001	14.030	14.027	14.072	14.042	14.173	19.853	19.909	19.961	13.963	14.013	19.851	19.865	14.024	13.991	13.995	14.014	14.017	19.826	14.036	19.801
X_{Mg}	0.561	0.496	0.947	0.956	0.882	0.887	0.862	0.839	0.815	0.833	0.942	0.926	0.968	0.968	0.988	0.953	0.975	0.975	0.947	0.978	0.943	0.977

X_{Mg} = Mg/(Mg + Fe)
Chl (1) first generation chlorite, Chl (2) second generation chlorite

Table 3 Thermodynamic properties at 298.15 K and 1 bar of end members used in this study

End member	Formula	$\Delta_f H°$ J mol^{-1}	$S°$ J mol^{-1} K^{-1}	$V°$ J mol^{-1} bar^{-1}	k_0	k_1	$k_2 \times 10^{-2}$	$k_3 \times 10^{-4}$	$v_1 \times 10^{+5}$ K^{-1}	v_2 K^{-2}	$v_3 \times 10^{+5}$ bar^{-1}	v_4 bar^{-2}	Source
Fe-carpholite	FeAl$_2$Si$_2$O$_6$(OH)$_4$	−4422380.00	248.700	10.690	620.648	−4928.62	−97484.2	155431.2	2.80636108	0	0.00000000	0	(1), (1), (2), (4), (5)
Mg-carpholite	MgAl$_2$Si$_2$O$_6$(OH)$_4$	−4772855.71	221.100	10.590	601.808	−4505.05	−111530.0	166142.7	2.92728989	0	−0.17941454	0	(1), (1), (2), (4), (5)
Fe-chloritoid	FeAl$_2$SiO$_5$(OH)$_2$	−3208718.33	162.000	6.980	426.537	−3182.81	−72198.6	109991.7	2.72206303	0	−0.10744986	0	(1), (1), (2), (4), (5)
Mg-chloritoid	MgAl$_2$SiO$_5$(OH)$_2$	−3556410.00	134.550	6.864	407.697	−2759.24	−86244.4	120709.2	3.00000000	0	−0.06760000	0	(1), (1), (3), (4), (6)
Daphnite	Fe$_5$Al$_2$Si$_3$O$_{10}$(OH)$_8$	−7140116.67	569.500	21.340	1229.233	−10256.49	−122769.8	212150.7	2.76476101	0	−0.17806935	0	(1), (1), (2), (4), (5)

Data sources: (1) $\Delta_f H°$ and S° from this study by optimisation, (2) $V°$ molar volume from Holland and Powell (1990), (3) $V°$ molar volume from Comodi et al. (1992), (4) Cp coefficients from oxide sum equation of Berman and Brown (1985), (5) v_1–v_4 expansivity and compressibility coefficients derived from the thermal expansion and compressibility coefficients of Holland and Powell (1990), (6) v_1–v_4 expansivity and compressibility coefficients calculated using the bulk modulus measured by Comodi et al. (1992) and expansivity measured by Ivaldi et al. (1988). $\Delta_f H°$ molar enthalpy of formation from the elements (J mol^{-1}), S° molar entropy (J mol^{-1} K^{-1}) and $V°$ molar volume (J mol^{-1} bar^{-1}) at standard state. k_0–k_3 $Cp(T)$ coefficients for the heat expression (J mol^{-1} K^{-1}): $Cp = k_0 + k_1 T^{-0.5} + k_2 T^{-2} + k_3 T^{-3}$ (notation of Berman 1988). v_1–v_4 expansivity and compressibility coefficients for the volume expression: $V(P,T)/V° = 1 + v_1(T-298.15) + v_2(T-298.15)^2 + v_3(P-1) + v_4(P-1)^2$ (modified notation of Berman 1988)

Alm + 2Crn + 3H$_2$O, and of Chopin and Schreyer (1983) for the reaction 5Mg-Cld ⇔ Cln + 2Crn + 2Ky + H$_2$O. $\Delta_f H°$ and S° for Mg-Car were retrieved from the experimental results of Chopin and Schreyer (1983) for the reactions 5Mg-Car ⇔ Cln + 4-Ky + 3Qtz + 6H$_2$O, 14Mg-Car ⇔ 3Mg-Tlc + Cln + 13Ky + 21H$_2$O, 3Mg-Car + Qtz ⇔ Mg-Tlc + 3Ky + 5H$_2$O and from the estimated P–T position of the reaction 5Mg-Car + 9Qtz ⇔ 4Prl + Cln + 2H$_2$O. The Fe-Car entropy was estimated according to Spear and Cheney (1989) by adding the FeMg$_{-1}$ exchange entropy (27.6 J mol^{-1} K^{-1}) to S°$_{Mg-Car}$. The Fe-Car enthalpy of formation was retrieved from the approximate location of the reaction Fe-Car ⇔ Fe-Cld + Qtz + H$_2$O from Chopin and Schreyer (1983). The enthalpy of formation and entropy of daphnite were retrieved from Fe–Mg partitioning for the equilibrium 5Alm + 3Cln ⇔ 5Prp + 3Dap by Dickenson and Hewitt (in Laird 1988) and 5Phl + 3Dap ⇔ 5Ann + 3Cln from Laird (1988). Our derived $\Delta_f H°$ and S° of daphnite tend to be approximate because they are retrieved from exchange reactions that have Fe–Mg partition coefficient K_D depending on the accuracy of the Al-, Fe- and Mg-content of chlorites as well as P and T estimations of the source data. As the element fractionation for these two exchange reactions happens to be such that ln K_D is strongly temperature dependent, the entropy and enthalpy changes for the exchange reactions ($\Delta_r S$ and $\Delta_r H$) are large. Consequently, the PTX conditions of these two exchange reactions are not very sensitive to small errors in our estimations of S° and $\Delta_f H°$ for daphnite. The heat capacity functions for daphnite, Fe- and Mg–chloritoid and carpholite (Table 3) were estimated from oxide sum calculations (Berman and Brown 1985), and their molar volume, thermal expansion and compressibility coefficients were taken from the literature (References are given in Table 3). Our thermodynamic data for the Mg-Cld are similar to those recently published (Vidal et al. 2001). The estimates of Holland and Powell (1990) for ferro-talc are used. These data are consistent within the limits of uncertainty with the observations of Chopin and Monié (1984), Miller (1986) and with this study for the reaction 3Mg-Cld + Fe-Tlc ⇔ 3Fe-Cld + Mg-Tlc.

The solution models used for the calculation of phase–assemblage diagrams are summarised in Table 4. The solution models for garnet and phengite are from Berman (1990) and Massonne and Szpurka (1997), respectively. Ideal Fe–Mg mixing on sites was assumed for biotite, carpholite, chlorite, chloritoid, cordierite, orthopyroxene and talc. Tschermak's substitution is ignored for the talc solution model because of the extremely low-Al content of talc occurring in magnesian metapelites (Table 2). A simple solid solution model for chlorite is based on an ideal Fe–Mg site distribution between daphnite and clinochlore although the compositions of measured chlorite are slightly more aluminous than clinochlore. The activity models proposed for chlorites by Holland et al. (1998) or more recently by

Table 4 Solution models used for the calculation of phase–assemblage diagrams

Mineral solution	Solution model
Biotite	Binary (Ann, Phl), site mixing, ideal $a_{Ann} = (X_{Fe}^M)^3$, $a_{Phl} = (X_{Mg}^M)^3$
Carpholite	Binary (Fe-Car, Mg-Car), site mixing, ideal $a_{Fe\text{-}Car} = (X_{Fe}^M)$, $a_{Mg\text{-}Car} = (X_{Mg}^M)$
Chlorite	Binary (Dap, Cln), site mixing, ideal $a_{Dap} = (X_{Fe}^M)^5$, $a_{Cln} = (X_{Mg}^M)^5$
Chloritoid	Binary (Fe-Cld, Mg-Cld), site mixing, ideal $a_{Fe\text{-}Cld} = (X_{Fe}^M)$, $a_{Mg\text{-}Cld} = (X_{Mg}^M)$
Cordierite	Binary (Fe-Crd, Mg-Crd), site mixing, ideal $a_{Fe\text{-}Crd} = (X_{Fe}^M)^2$, $a_{Mg\text{-}Crd} = (X_{Mg}^M)^2$
Garnet	Binary (Alm, Prp), site mixing, nonideal after Berman (1990)
Orthopyroxene	Binary (Fs, En), site mixing, ideal $a_{Fs} = (X_{Fe}^M)^2$, $a_{En} = (X_{Mg}^M)^2$
Phengite	Ternary (Ms, Cel, Fe-Cel), nonideal after Massonne and Szpurka (1997)
Talc	Binary (Fe-Tlc, Mg-Tlc), site mixing, ideal $a_{Fe\text{-}Tlc} = (X_{Fe}^M)^3$, $a_{Mg\text{-}Tlc} = (X_{Mg}^M)^3$

Cln clinochlore, *Cel* celadonite, *Fe-Cel* ferro-celadonite
Ideal is used in the sense of $a_i = (X_i^M)^n$ where a_i is the activity of the end member i in a given crystalline phase for which mixing occurs over only a single crystallographic site M, X_i is the mole fraction of the end member i and n is the site multiplicity of M. All other solution models are called nonideal

Vidal et al. (2001) cannot be used in a Gibbs free energy minimisation. These two activity models use end members (or proportions) that do not span the compositional space. In order to reach e.g. Fe-amesite, one of the proportions becomes negative, which is not supported in our Gibbs free energy minimisation. Furthermore, Holland et al. (1998) and Vidal et al. (2001) assume that there is no Mg or Fe partitioning between M1 and (M2 + M3) crystallographic sites for the calculation of the proportions. A G-minimisation will however result in such a partitioning because $(Fe/Mg)_{M1}$ and $(Fe/Mg)_{M2+M3}$ are calculated from the sum of the contributions of the end members. This contradiction yields undefined gradients for the minimisation.

For any interpretations of our calculated phase–assemblage diagrams, we estimate that absolute uncertainty for the position of individual phase assemblage boundaries are ± 2–3 kbar and $\pm 30°C$.

Model magnesian metapelites

For the calculations we focussed on magnesian metapelites with bulk composition comprised over 98.5% of weight percentages of the constituent oxides by the system KFMASH. Furthermore, these samples of natural magnesian metapelites with low TiO_2, MnO, CaO, Na_2O and P_2O_5 contents were chosen because of the detailed petrological and geochemical data existing in the literature and in this study. The selected natural magnesian metapelites come from the Monte Rosa, Gran Paradiso and Dora Maira nappes (Western Alps). The whole-rock chemical analyses for the samples are given in Table 1. Most major minerals in the magnesian metapelites can be described within the system K_2O–FeO–MgO–Al_2O_3–SiO_2–H_2O, whereas many of the minor minerals are stabilised by small amounts of calcium, sodium, manganese, titanium, phosphorus, sulphur, and rare-earth elements. Our simplified model magnesian metapelites are all contained within the system KFMASH (Table 5).

The 17 rock compositions investigated in this study are plotted in an AFM projection (Thompson 1957) in Fig. 3. Each sample contains quartz and potassic white mica. From Fig. 3 two main rock-composition populations may be recognised: one with a high- and one with a low-Al content. The low- and high-Al average bulk compositions (LAL and HAL, respectively) were calculated for both magnesian metapelite population (Fig. 3, Table 5). The LAL and HAL model compositions have approximately the same FeO/(FeO + MgO) ratio (0.246 and 0.227, respectively) but different values for the effective Al content X_A equal to 0.2130 and 0.4264, respectively. LAL is representative of the low effective Al content chloritoid-bearing magnesian

Table 5 Model bulk compositions for magnesian metapelites

Model	LAL	LALM	LALF	HAL	HALM	HALF
SiO_2 wt.%	Excess	Excess	Excess	Excess	Excess	Excess
Al_2O_3	59.24	62.52	52.61	56.71	61.62	48.68
FeO	5.25	0.00	15.86	7.97	0.00	20.99
MgO	17.85	18.84	15.86	24.46	26.57	20.99
K_2O	17.66	18.64	15.68	10.87	11.81	9.33
H_2O	Excess	Excess	Excess	Excess	Excess	Excess
Total	100.00	100.00	100.00	100.00	100.00	100.00
A = Al_2O_3–3K_2O%	21.30	21.30	21.30	42.64	42.64	42.64
F = FeO%	17.89	0.00	39.35	14.10	0.00	28.68
M = MgO%	60.81	78.70	39.35	43.26	57.36	28.68
A + F + M%	100.00	100.00	100.00	100.00	100.00	100.00
FeO/(FeO + MgO)	0.227	0.000	0.500	0.246	0.000	0.500

LAL average of low-Al population, *LALM* Mg end member of low-Al population, *LALF* intermediate FeO/(FeO + MgO) ratio (0.5) model composition for the low-Al population, *HAL* average of high-Al population, *HALM* Mg end member of high-Al population and *HALF* intermediate FeO/(FeO + MgO) ratio (0.5) model composition for the high-Al population
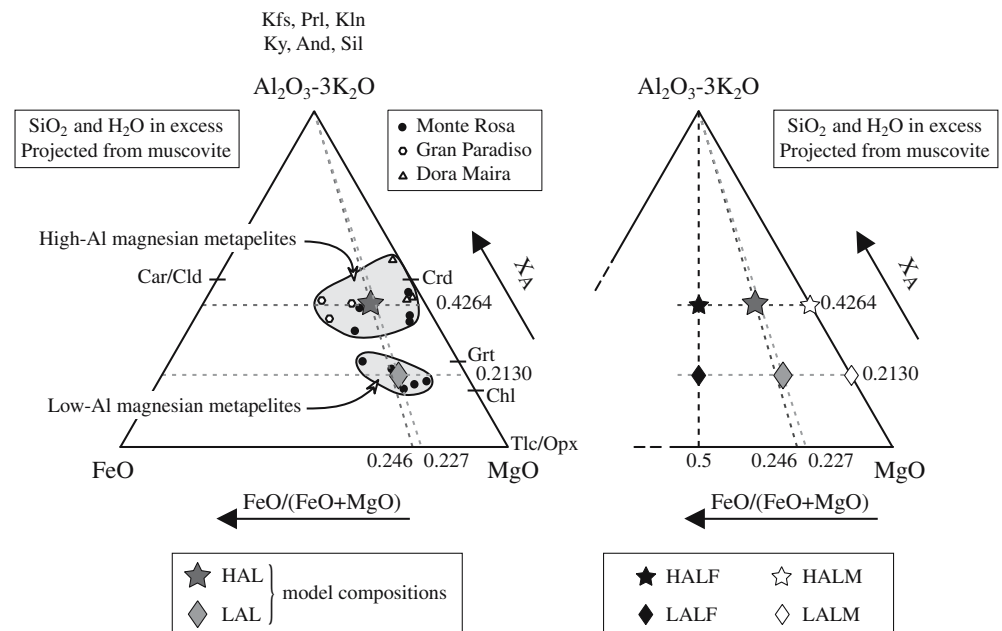
Table 6 Equilibrated mineral assemblages shown in Figs. 4, 5, 6, 7 and 8 with H₂O and Qtz/Cs (Cs = coesite)

	Mineral assemblage		Mineral assemblage
1	Prl + Chl + Phe	29	Chl + And + Phe
2	Tlc + Car + Chl + Phe	30	Opx + Crd + Bt
3	Cld + Tlc + Car + Phe	31	Opx + Grt + Crd + Bt
4	Cld + Tlc + Ky + Phe	32	Opx + Grt + Ky + Phe
5	Cld + Car + Chl + Phe	33	Opx + Grt + Sil + Bt
6	Cld + Chl + Ky + Phe	34	Opx + Ky + Phe
7	Tlc + Chl + Ky + Phe	35	Opx + Sil + Bt
8	Cld + Chl + Phe	36	Opx + Tlc + Ky + Phe
9	Crd + Bt + Phe	37	Opx + Crd + Tlc + Bt
10	Crd + Chl + Phe	38	Opx + Grt + Ky + Bt
11	Chl + Ky + Bt	39	Crd + And + Bt
12	Chl + Sil + Bt	40	Crd + Kfs + Bt
13	Crd + Sil + Bt	41	Crd + Tlc + Bt
14	Tlc + Sil + Bt	42	Grt + Chl + Ky + Phe
15	Grt + Tlc + Ky + Bt	43	Grt + Cld + Chl + Phe
16	Grt + Tlc + Sil + Bt	44	Grt + Cld + Tlc + Phe
17	Tlc + Ky + Phe	45	Grt + Crd + Tlc + Bt
18	Sil + Phe + Bt	46	Grt + Chl + Ky + Bt
19	Kfs + Sil + Bt	47	Grt + Ky + Phe + Bt
20	And + Phe + Bt	48	Grt + Ky + Kfs + Bt
21	Tlc + Ky + Phe + Bt	49	Grt + Opx + Ky + Phe
22	Chl + And + Bt	50	Grt + Opx + Ky + Kfs
23	Crd + Opx + Kfs	51	Grt + Ky + Kfs
24	Chl + Sil + Phe	52	And + Kfs + Bt
25	Tlc + Car + Ky + Phe	53	Opx + Ky + Kfs
26	Car + Phe	54	Opx + Ky + Bt
27	Tlc + Cld + Chl + Phe	55	Grt + Sil + Bt
28	Prl + Cld + Chl + Phe	56	Chl + Kfs + Phe

metapelites of the Monte Rosa nappe. Four additional model compositions—LALM, LALF, HALM and HALF—are also defined (Table 5). These are used, in conjunction with the LAL and HAL compositions, to examine the effect of whole-rock FeO/(FeO + MgO) ratio on the sequence of mineral assemblages. LALM and HALM are the Mg end member model compositions for the low- and high-Al magnesian metapelites.

LALF and HALF are the intermediate FeO/(FeO + MgO) ratio (0.5) model compositions for the low- and high-Al magnesian metapelites. Model compositions HALF and HALM are similar to the high-Al magnesian metapelite bulk compositions of the high-Fe sample 7–20b (Table 1) from the Gran Paradiso nappe and the Mg-rich sample 17641 (Table 1) from the coesite-bearing unit of the Dora Maira massif.

Fig. 3 Mineral, whole-rock (Table 1) and model (Table 5) compositions used in this study and plotted in the Thompson AFM (+ K-mica + SiO₂ + H₂O) projections. HAL (*grey star*) and LAL (*grey diamond*) refer to the model compositions (Table 5) used for high-Al and low-Al magnesian metapelites, respectively. HALM (*white star*) and LALM (*white diamond*) are the Mg end member model compositions for HAL and LAL. HALF (*black star*) and LALF (*black diamond*) are the intermediate FeO/(FeO + MgO) ratio (0.5) model compositions for HAL and LAL

Model calculations have also been carried out for several samples of natural magnesian metapelite of the Monte Rosa, Gran Paradiso and Dora Maira nappes in order to compare the mineral assemblages predicted for a specific bulk rock composition with mineral assemblages actually observed in the rock.

Petrologic particularities highlighted by phase–assemblage diagrams with a(H₂O) = 1

Phase–assemblage diagrams calculated with a(H₂O) = 1 for the bulk compositions of the Monte Rosa magnesian metapelites with SiO_2 and H_2O in excess do not show any of the typical assemblages occurring in natural magnesian metapelites such Cld–Tlc–Phe–Qtz (e.g. 99MR107—Fig. 2a) and/or Tlc–Ky–Phe–Qtz (e.g. 99MR56—Fig. 2e) at any geologically valid P–T conditions. Two reasons may be advanced to explain the absence of such typical assemblages. The first reason is that the water activity is much lower than 1. High pressure aqueous fluid involved in dehydration reactions is commonly assumed as pure H_2O. Hydration reactions are usually shifted down-temperature with decreasing a(H₂O). A reduced water activity at HP conditions in magnesian metapelites has been shown by Chopin (1984), Chopin and Monié (1984) and by Sharp et al. (1993). The second reason is that the bulk compositions used for the calculations do not correspond to the effective bulk composition of the rock. The magnesian metapelites have a wide range of bulk compositions (Table 1) and the observed minerals are not always homogeneous (Table 2). The effects of the water activity and bulk composition variations on the mineral assemblage stability are discussed in the following.

Effects of variable a(H₂O)

Phase diagrams of temperature and pressure versus water activity at 24 kbar and 500°C, respectively, are shown for the LAL model in Fig. 4. A list of labelled assemblages is given in Table 6. The minimum temperature of 450°C was chosen because lower temperature conditions are unrealistic at such high pressure conditions.

Figure 4 shows that a(H₂O) has a major effect on the calculated stabilities of the mineral assemblages at specific P–T conditions in magnesian metapelites. Quantitative data are discussed here only for the characteristic HP assemblage Cld–Tlc–Phe–Qtz, occurring in the Monte Rosa magnesian metapelites for which LAL is representative, to illustrate the dependency of its stability on a(H₂O).

With reducing a(H₂O) at 500°C and 24 kbar (Fig. 4a) the mineral sequence with excess SiO_2 and H_2O is: Chl–Car–Phe/Chl–Cld–Phe/Cld–Tlc–Phe/Cld–Tlc–Ky–Phe/Grt–Tlc–Ky–Phe/Grt–Ky–Phe ± Bt.

With reducing a(H₂O) in the LAL model at pressures between 20 and 25 kbar and at 500°C (Fig. 4b), the progressive appearance of chlorite, carpholite, chloritoid, talc, kyanite, garnet and biotite is associated with the following sequence (with excess SiO_2 and H_2O): Chl–Car–Phe/Chl–Cld–Phe/Cld–Tlc–Phe/Cld–Tlc–Ky–Phe/Grt–Tlc–Ky–Phe/Grt–Ky–Bt–Phe. At pressures between 10 and 15 kbar the mineral sequence with decreasing a(H₂O) consists of Chl–Phe/Chl–Ky–Phe/Chl–Ky–Tlc–Phe/Ky–Bt–Phe/Ky–Bt–Kfs/Ky–Opx–Kfs. With reducing a(H₂O) at 500°C and below 5 kbar Chl–Bt–Phe is replaced by Crd–Bt–Kfs and then by Crd–Opx–Kfs.

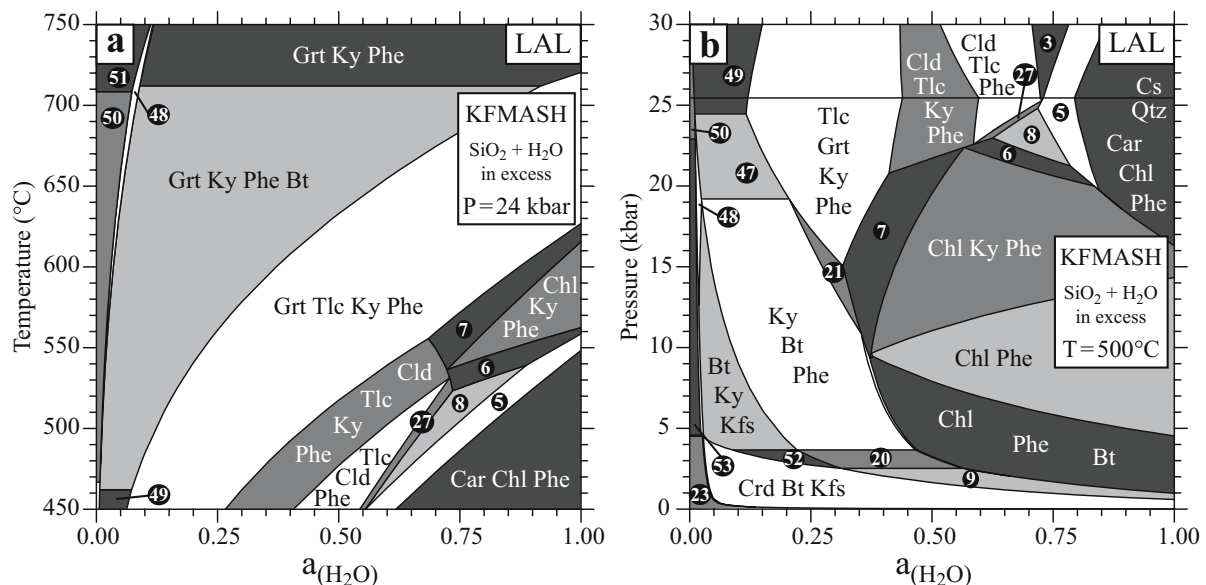Fig. 4 a T–a(H₂O) phase–assemblage diagram calculated for LAL at a pressure of 24 kbar with SiO_2 and H_2O in excess. b P–a(H₂O) phase–assemblage diagram calculated for LAL at a temperature of 500°C with SiO_2 and H_2O in excess
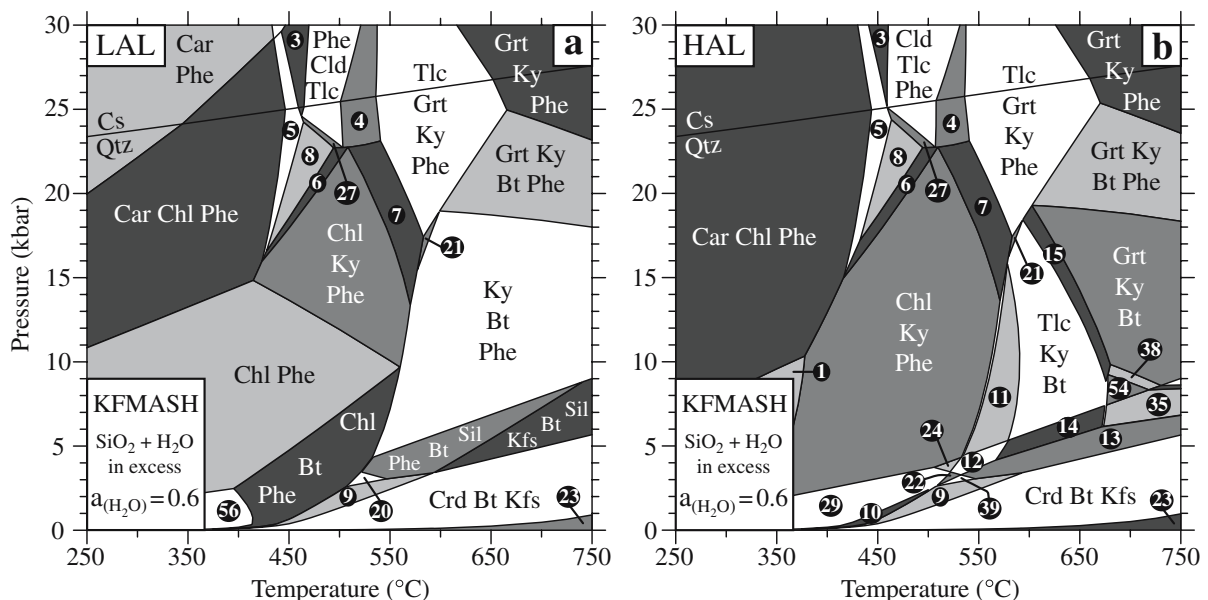
According to the phase–assemblage diagrams (Fig. 4), the occurrence of the Cld–Tlc–Phe–Qtz assemblage is restricted to an a(H$_2$O) between 0.59 and 0.66 at 24 kbar and 500°C. This characteristic assemblage, typically present in magnesian metapelites (e.g. in the Monte Rosa nappe), is shown to be very sensitive to a(H$_2$O). It is suggested that its appearance in natural rocks is due to the reduction of a(H$_2$O). This is supported by the work of Chopin and Monié (1984) who have measured a(H$_2$O) equal to 0.6 at HP in magnesian metapelites from the Furgg unit (Monte Rosa massif, Western Alps). Sharp et al. (1993) have also shown in an isotopic study that a(H$_2$O) must be reduced and lie between 0.4 and 0.75 at 700–750°C and 34 ± 2 kbar for the coesite-pyrope-bearing magnesian metapelites from the Dora Maira massif (Western Alps). These authors concluded that a decrease of water activity could result from a slab-derived fluid interacting with the surrounding gneiss. They compare this fluid with the K, Mg, Si-rich fluids/partial melts forming at high pressures and low temperatures described by Schreyer et al. (1987) and Massonne (1992). These fluids were observed in the experimentally studied breakdown reactions of phlogopite in the presence of K-feldspar and/or SiO$_2$ in the synthetic system KMASH. An average a(H$_2$O) of 0.6 is used for further calculations of phase–assemblage diagrams in the following sections.

P–T phase–assemblage diagrams with a(H$_2$O) = 0.6 for LAL and HAL

P–T phase–assemblage diagrams for LAL (low-Al model composition) and HAL (high-Al model composition) have been calculated with fixed a(H$_2$O) of 0.6 (Fig. 5) with excess SiO$_2$ and H$_2$O.

At low to medium *P–T* conditions, the higher effective Al content of HAL stabilises the mineral associations Prl–Chl–Phe, Chl–And–Phe, Chl–Ky–Phe, and Car–Chl–Phe rather than Chl–Kfs–Phe, Chl–Bt–Phe and Chl–Phe, which occur in LAL. The high-X_A content of HAL stabilises the Prl–Chl–Phe assemblage at LP–LT and increases the stability field of the Car–Chl–Phe and Chl–Ky–Phe assemblages towards lower pressures. These three mineral associations are replaced by the Chl–Phe assemblage in LAL at low temperature and low to medium pressure conditions. At medium temperatures, the stability field of the Chl–Ky–Phe assemblage expands to lower pressures in HAL replacing the Chl–Phe and Chl–Bt–Phe assemblages occurring in LAL. At LP–MT, the low-X_A content of LAL stabilises the mineral associations Chl–Kfs–Phe and Chl–Bt–Phe rather than Chl–And–Phe that is stable in HAL. At LP–HT, the Crd–Bt–Kfs assemblage occurs for both model compositions. The difference between LAL and HAL in the sequence of mineral assemblages at medium to high pressure and temperature conditions is the appearance in HAL of talc and then garnet in a Ky–Bt bearing assemblage during prograde metamorphism, while in LAL phengite is still stable in a mineral assemblage consisting of Ky–Bt–Phe. In contrast, the predicted mineral associations at high pressure are less dependent on the X_A variations as LAL and HAL show a similar sequence of mineral assemblages. Above 20 kbar, the prograde sequence of mineral assemblages is: Car–Chl–Phe → Chl–Cld–Phe → Cld–Tlc–Phe → Cld–Tlc–Phe–Ky → Tlc–Grt–Ky–Phe → Grt–Ky–Phe ± Bt.

LAL corresponds roughly to the average composition of the low effective Al content magnesian metapelites found in the Monte Rosa. While the phase–assemblage diagram calculated for LAL with a reduced a(H$_2$O)

Fig. 5 *P–T* phase–assemblage diagrams calculated for LAL (**a**) and HAL (**b**) with fixed a(H$_2$O) of 0.6 with SiO$_2$ and H$_2$O in excess

displays, at high pressures, the observed assemblage Cld–Tlc–Phe, the phase–assemblage diagram calculated for HAL with a reduced a(H₂O) does not display any other typical assemblages found in natural magnesian metapelites such as Tlc–Ky–Phe or Chl–Ms. The Tlc–Ky–Phe assemblage is only stable in very magnesium rich systems for which HAL and LAL are not representative. The Chl–Ms assemblage occurs in both low- and high-X_A natural magnesian metapelites of the Monte Rosa nappe. Because the Chl–Ms assemblage is predicted to be only stable for LAL, part of the Al bound in kyanite is suspected to be isolated from a more Al-poor effective bulk composition. In order to investigate how strong the Fe and Al contents influence the stable assemblages, phase–assemblage diagrams were calculated for different Al contents and varying Fe/(Fe + Mg) ratios.

Effects of FeO/(FeO+MgO) ratio and X_A content

In order to focus attention on the changes in equilibrium mineral assemblages with variations in P, T and X, phase–assemblage diagrams were calculated for an effective Al content X_A at constant temperature with pressure versus FeO/(FeO + MgO). Calculated diagrams using original LAL and HAL model compositions at 500°C, 650°C and a(H₂O) = 0.6, are shown in Figs. 6 and 7. The range of the FeO/(FeO + MgO) is defined by the different model compositions LALF, LALM, HALF and HALM (Table 5).

In both 500°C diagrams of P versus FeO/(FeO + MgO) (Fig. 6a, b), critical whole-rock MgO contents are required to stabilise Cld–Chl–Phe, Cld–Tlc–Phe, Cld–Tlc–Ky–Phe and Tlc–Ky–Phe assemblages with SiO₂

and H₂O in excess at high pressures. The Tlc–Ky–Phe assemblage only appears in a nearly iron-free system. The whole-rock FeO/(FeO + MgO) ratio plays a critical role in determining the pressure at which chloritoid and talc first appear in magnesian metapelites during metamorphism (Fig. 6). In contrast, the first appearance of andalusite, phengite, chlorite, kyanite or the disappearance of potassic feldspar, cordierite, biotite with increasing pressure at 500°C are relatively independent of whole-rock FeO/(FeO + MgO) ratio (Fig. 6).

In the P versus FeO/(FeO + MgO) diagram at 650°C (Fig. 7), a critical FeO/(FeO + MgO) ratio is required to stabilise Grt–Ky–Phe, Grt–Tlc–Ky–Phe and Tlc–Ky–Phe assemblages at high to very high pressures. The Tlc–Ky–Phe assemblage is restricted to nearly iron-free bulk compositions. At medium pressures the stability fields of Grt–Ky–Phe–Bt, Ky–Phe–Bt, Grt–Ky–Bt and Tlc–Ky–Bt are strongly dependent on the FeO/(FeO + MgO) ratio of the rock. At low pressures the stability field of the Crd–Kfs–Bt assemblage is not affected by FeO/(FeO + MgO) variations.

The P versus FeO/(FeO + MgO) diagram calculated for LAL and HAL at 500°C (Fig. 6) may also be used to estimate the influence of the effective Al content on the mineral assemblages. As already predicted in the P–T phase–assemblage diagrams (Fig. 5), the stability of the assemblages Chl–Phe–Bt, Chl–Phe, Chl–Ky–Phe with SiO₂ and H₂O in excess is very sensitive to the bulk X_A. The pressure dependence of the Chl–Bt–Phe and Chl–Phe stability on whole-rock effective Al content is shown by the marked expansion of the Chl–Ky–Phe field towards low pressures in HAL compared to LAL. On the other hand, the high pressure assemblages are less sensitive to X_A variations.
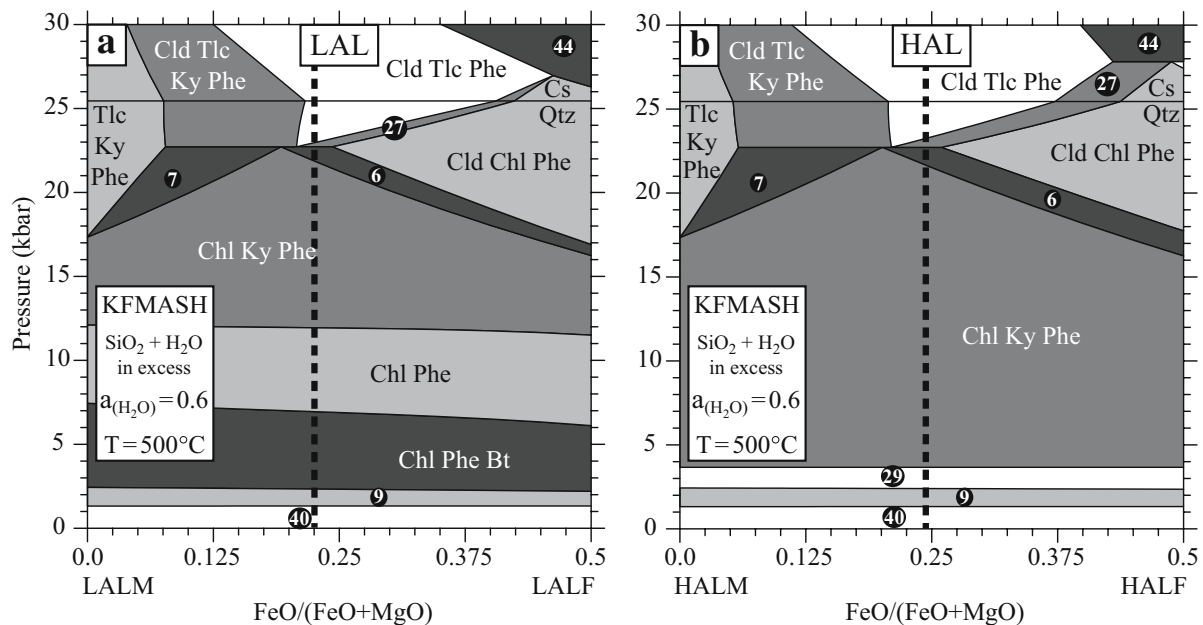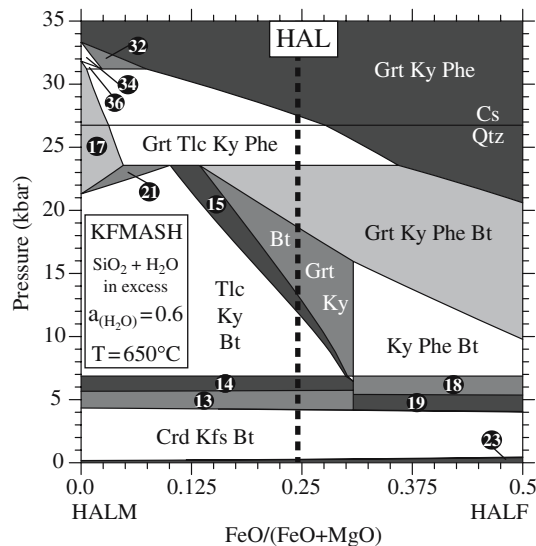

Fig. 6 Binary P versus FeO/(FeO + MgO) phase–assemblage diagrams calculated around LAL (**a**) and HAL (**b**) with fixed a(H₂O) of 0.6 at 500°C with SiO₂ and H₂O in excess. LAL and HAL are indicated by the *dashed vertical line*

Fig. 7 Binary P versus $FeO/(FeO + MgO)$ phase–assemblage diagram calculated around HAL (indicated by the *dashed vertical line*) with fixed $a(H_2O)$ of 0.6 at 650°C with SiO_2 and H_2O in excess

The results presented in Figs. 6 and 7 emphasise the importance of the bulk-rock composition on the appearance of typically observed mineral assemblages in magnesian metapelites.
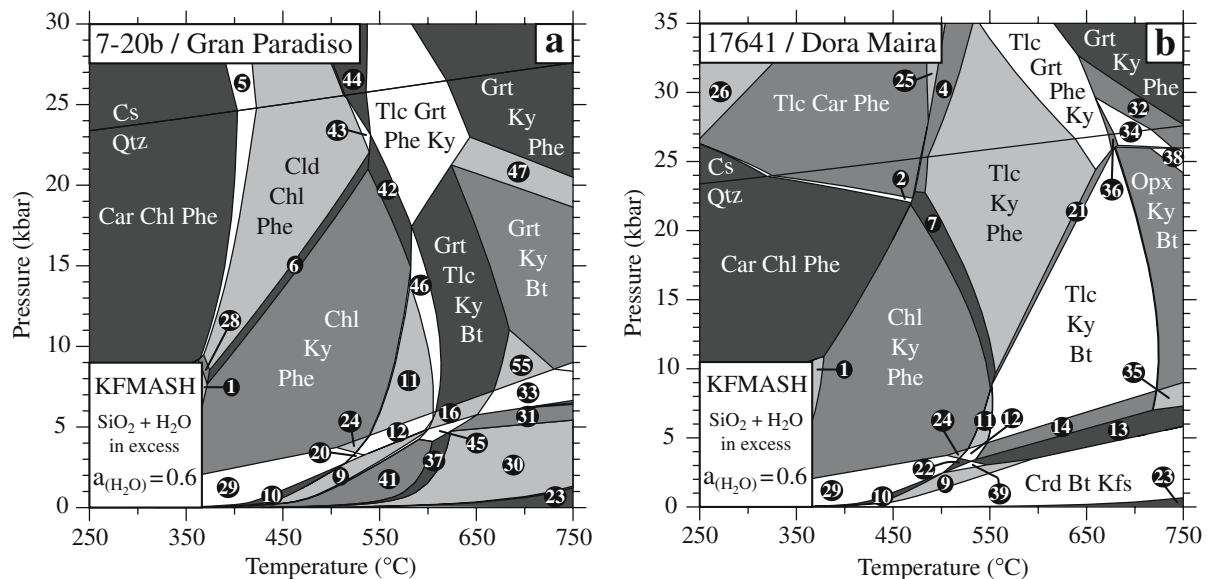
Phase–assemblage diagrams for HALF and HALM

As illustrated above, $FeO/(FeO + MgO)$ ratio and X_A content in the bulk-rock composition are critical for the development of the naturally occurring mineral assemblages under given P–T conditions. Phase–assemblage

diagrams for the samples 7–20b (from the Gran Paradiso nappe) and 17641 (from the Dora Maira nappe) are calculated with fixed $a(H_2O)$ of 0.6 in order to document how phase relations respond in the high effective Al magnesian metapelites to $FeO/(FeO + MgO)$ ratio and variation in pressure and temperature (Fig. 8). The bulk compositions of the samples 7–20b and 17641 are very similar to HALF and HALM, respectively.

The phase diagram calculated for the composition 7–20b (Fig. 8a) is similar to HAL (Fig. 5b) except at LP–HT conditions where the Crd–Bt–Opx and Crd–Bt–Tlc assemblages replace the Crd–Bt–Kfs assemblage. The higher Fe content in 7–20b expands the Grt–Ky–Phe assemblage towards lower P–T conditions at the expense of the Tlc–Grt–Ky–Phe and Grt–Ky–Bt–Phe assemblages at HP–HT and stabilises the Grt–Tlc–Ky–Bt assemblage at MP–HT. The Cld–Tlc–Phe ± Ky assemblage occurring in HAL at HP–MT (Fig. 5b) is replaced by the Grt–Cld–Tlc–Phe and Cld–Chl–Phe assemblages in 7–20b (Fig. 8a). In addition, the stability field of the Cld–Chl–Phe assemblage at HP-MT expands compared to HAL (Fig. 5b) towards lower P and T at the expense of the Car–Chl–Phe and Chl–Ky–Phe mineral assemblages.

For the sample 17641 (Fig. 8b), the mineral assemblages at low to medium temperatures are similar to the HAL composition. As already predicted in the binary phase–assemblage diagram P versus $FeO/(FeO + MgO)$ ratio (Fig. 6), the Tlc–Ky–Phe assemblage is only stable in iron-free systems with SiO_2 and H_2O in excess. Consequently, the stability field of the Tlc–Ky–Phe assemblage appears at moderate to high P–T conditions in sample 17641 at the expense of the chloritoid–talc–phengite association and the chloritoid–phengite and kyanite–phengite bearing assemblages associated with

Fig. 8 P–T phase–assemblage diagrams calculated for the samples 7–20b from the Gran Paradiso (**a**) and 17641 from the Dora Maira (**b**) with fixed $a(H_2O)$ of 0.6 with SiO_2 and H_2O in excess

chlorite, garnet and biotite occurring in HAL. Toward higher temperatures, phengite occurring in the Tlc–Ky–Phe assemblage breaks down to phlogopite in a mineral assemblage consisting of Tlc–Ky–Bt. Above ~700°C, talc is predicted to be replaced by enstatite in the Opx–Ky–Bt assemblage at moderate to high pressures. With increasing $P–T$ conditions, talc occurring in the Tlc–Grt–Ky–Phe assemblage at UHP–HT breaks down to enstatite in the Opx–Grt–Ky–Phe assemblage or garnet in the Grt–Ky–Phe assemblage at higher pressures.

Comparison and application to natural magnesian metapelites from the Western Alps

Well-documented geological observations on natural magnesian metapelites from the Gran Paradiso, Dora Maira and Monte Rosa nappes are compared with phase–assemblage diagrams for magnesian metapelites. The applicability of the calculated phase–assemblage diagrams lies in the ability to account for observed mineral parageneses and to help explain their textural relations.

Magnesian metapelites from the Gran Paradiso nappe

The Gran Paradiso internal massif consists of ortho- and paragneisses interbedded with metabasites and pelitic schists and intruded by porphyritic granites all of which were subjected to an Alpine high pressure metamorphic event (Chopin 1981; Vearncombe 1983; Dal Piaz and Lombardo 1986). Because of their structural

Fig. 9 Compilation of calculated $P–T$ phase–assemblage diagrams and proposed $P–T$ path for different investigated magnesian metapelites of the Monte Rosa nappe with fixed a(H$_2$O) of 0.6 at high pressure and of 1.0 at low pressure with SiO$_2$ and H$_2$O in excess

and petrographical similarities, the Monte Rosa and Gran Paradiso nappes are commonly assumed to have the same origin. Using whole-rock compositions given by Chopin (1979, 1981), phase–assemblage diagrams have been calculated in order to compare them with the natural assemblages and to provide $P–T$ data for the high pressure event occurring in the Gran Paradiso nappe. In sample 7–37 (Chopin 1981), a chloritoid–talc–phengite–quartz assemblage and in samples 7–20b and 6–298a (Chopin 1979) a chloritoid–garnet–talc–phengite–quartz assemblage are reported in magnesian metapelites which were found in the Gran Paradiso basement. For the reasons explained above, a(H$_2$O) is fixed at 0.6 and the small amounts of MnO, CaO, Na$_2$O and TiO$_2$ are neglected. In our phase–assemblage diagram calculations for sample 7–20b (Fig. 8a), a small high pressure stability field for the observed natural assemblage Cld–Tlc–Grt–Phe–Qtz is found around 24 kbar and 525°C. This is considered to be the Alpine peak of high pressure metamorphism in the Gran Paradiso massif. The phase diagrams confirm the importance of specific mineral assemblages to constrain P and T and show a good agreement between our thermodynamic prediction and the observed mineral assemblages.

Magnesian metapelites from the coesite-bearing unit of the Dora Maira massif

For further tests on the validity of our thermodynamic database, calculations were done with the coesite-bearing magnesian metapelites from the Dora Maira nappe (Western Alps) equilibrated under very high pressure conditions. Phase relations involving garnet, talc, kyanite, phengite and SiO$_2$ in the system KFMASH have been described by Chopin (1984, 1991) and Schertl et al. (1991) for a pyrope-coesite-quartzite of the Dora Maira massif. To compare our calculated modelling with the natural mineral assemblages and with previous $P–T$–a(H$_2$O) data (Chopin 1984; Sharp et al. 1993), a phase–assemblage diagram has been calculated using the whole-rock composition of sample 17641 from Tilton et al. (1991) and a(H$_2$O) = 0.6 (Fig. 8b). Modelling predicts a similar mineral sequence to the one observed by Schertl et al. (1991) at HP with increasing temperature and pressure. This sequence is (with SiO$_2$ and H$_2$O in excess): Chl–Ky–Phe → Tlc–Ky–Phe → Tlc–Ky–Grt–Phe → Ky–Grt–Phe.

Sharp et al. (1993) estimated the temperatures for the observed assemblage Tlc–Ky–Grt–Phe to be between 700 and 750°C based on δ^{18}O quartz–garnet–rutile fractionation. Our thermodynamic calculations predict this assemblage at temperatures about 100°C lower. Besides uncertainties in thermodynamic data, this discrepancy may stem from uncertainties in the effective bulk composition because of partial equilibrium (e.g. Loomis 1983; Spear 1988; Hetherington and Le Bayon 2005). Because most of the Fe is fractionated into gar-

net, it does not take part in later equilibria and thus the effective bulk composition becomes almost iron-free. Figure 7 demonstrates that the transition between the assemblages Tlc–Ky–Grt–Phe and Ky–Grt–Phe depends strongly on the FeO/(FeO + MgO) ratio. Fractionation of Fe in garnet will lower the effective FeO/(FeO + MgO) ratio and thus stabilise the assemblage Tlc–Ky–Grt–Phe rather than the assemblage Grt–Ky–Phe at the UHP–HT conditions in the magnesian metapelites of the Dora Maira massif.

With the exception of possible Fe fractionation in garnet, the modelling produces results compatible with the mineral assemblages observed in the Dora Maira samples during the prograde metamorphism (Fig. 8b).

Magnesian metapelites from the Monte Rosa nappe

Magnesian metapelites from the roof of the Monte Rosa nappe provide an ideal opportunity to compare calculated predictions with observed mineral assemblages in natural rock samples and to reconstruct their P–T history.

The whole-rock composition is used to calculate a phase–assemblage diagram with a(H$_2$O) = 0.6 for the high pressure part of the metamorphic evolution assuming that the rock was completely and homogeneously equilibrated. Several phase–assemblage diagrams were calculated for different magnesian metapelites and are compiled in a single P–T diagram showing the stability fields of common mineral assemblages (Fig. 9). The stability field of the characteristic assemblage talc–magnesiochloritoid associated with phengite, given a water activity of 0.6, is constrained to approximately 24 kbar and temperatures around 505 ± 30°C. This is considered to be the peak of Alpine eclogite facies metamorphism in this area. The upper pressure limit (at ~26 kbar) is given by the quartz–coesite transition. The lower pressure limit is estimated at around 20 kbar considering absolute pressure uncertainty of 2–3 kbar for the position of individual phase assemblage boundaries.

For the intermediate pressure assemblages resulting from the breakdown of high pressure mineral assemblages, it is less reliable to use the original bulk composition because the high pressure mineral relics, which did not react during post-HP peak of metamorphism, affect the effective bulk composition. To calculate the stability field of the assemblage Ky–Chl–Phe, only the Mg-rich and nearly iron-free metapelite whole-rock compositions were used because they preserved completely re-equilibrated intermediate pressure assemblages. A common P–T stability field (Fig. 9) is located at pressures and temperatures ranging between 11–21 kbar and 430–540°C. The talc inclusions in kyanite crystals demonstrate that talc in the matrix is completely consumed during decompression (Fig. 9). Chlorite appears as a result of talc breakdown. This demise constrains the decompression path between

an approximate P–T range of 21 kbar/480°C and 13 kbar/540°C.

The late metamorphic assemblage of Chl–Ms occurs in completely re-homogenised rocks and as small subsystems like pressure shadows or breakdown locations of high pressure metamorphic minerals. For rocks showing a complete late re-equilibration, their whole-rock compositions were used. In other cases we measured bulk compositions of the equilibrated late assemblage in local breakdown locations by EDS analysis with the electron microprobe. These late retrograde assemblages made of chlorite-muscovite with excess quartz replaced chloritoid, talc, chlorite and kyanite (Fig. 2b–e). As some of the Chl–Ms assemblages occur in pressure shadows and are aligned in the foliation (Fig. 2e) and some others are undisturbed by the deformation (Fig. 2c–d), they are labelled in Fig. 9 as "Chl-Ms (deformed)" and "Chl-Ms (undeformed)". Because water-rich fluid inclusions are observed in phases of the late recrystallisation, a(H$_2$O) is fixed to unity to calculate phase–assemblage diagrams for the late metamorphic event. The compiled results are shown in Fig. 9. The magnesian metapelites experienced a decompression below ~8 kbar and ~ 475°C with concomitant cooling during a further retrogression when the late chlorite–muscovite assemblage locally grew or completely obliterated high pressure minerals.

A complete P–T exhumation path of the Monte Rosa nappe is obtained from the succession of P–T stability fields for mineral assemblages in the magnesian metapelites (Fig. 9). The path is divided in two parts: a first near-isothermal decompression from around 24 kbar and 505°C to 8 kbar and 475°C, followed by a second decompression with concomitant cooling. The P–T path reveals two different exhumation regimes where different tectonic deformations occurred (R. Le Bayon et al., in preparation). Considerable insight into the P–T path of the Monte Rosa nappe is gained using the method of phase–assemblage diagram calculations. The fundamental similarity of the Alpine high pressure metamorphic climax of the Monte Rosa and Gran Paradiso nappes supports the possible structural connection between these two internal massifs. Furthermore, they may have the same palinspastic origin as suggested by lithologic, structural and deep seismic arguments (Dal Piaz and Lombardo 1986; Schmid and Kissling 2000). In the present study, we did not detect any Barrovian overprint by the late Lepontine metamorphism in the western roof of the Monte Rosa nappe.

Conclusions

Calculations of phase–assemblage diagrams can adequately model typical assemblages in ultra-high, high, medium and low pressure and temperature conditions for Mg-rich metapelites in the system KFMASH. The expected uncertainties of the equilibrium assemblage boundaries are ±3 kbar and ±30°C. Results reported

here emphasise the importance of a(H$_2$O), effective bulk composition (FeO/(FeO + MgO) ratio and X_A content), as well as physical environment (pressure and temperature) on the stability of mineral assemblages. The mineral assemblages predicted in the calculated phase–assemblage diagrams are consistent with the well-established petrological observations. Taking into account the effective bulk composition and a(H$_2$O) involved in the metamorphic history, phase–assemblage diagrams similar to those presented in this study may be calculated for any magnesian metapelites with composition bounds in the system KFMASH.

These diagrams are useful tools for elucidating the P–T path of magnesian metapelites-bearing tectonic terranes. In the present study the P–T conditions of the exhumation path for the top of the Monte Rosa nappe have been derived from such magnesian metapelites. The exhumation shows first a near-isothermal decompression from the alpine eclogite peak conditions around 24 kbar and 505°C down to approximately 8 kbar and 475°C followed by a second decompression with concomitant cooling. Furthermore, the derived metamorphic history strengthens the lithological, structural and deep seismic arguments that the Monte Rosa and Gran Paradiso nappes are the same tectonic unit.

Appendix

Table 7 Experimental and approximate brackets used for deriving $\Delta_f H°$ and $S°$ of Fe-chloritoid, Mg-chloritoid, Mg-carpholite and Fe-carpholite by optimisation

Label	P (bar)	T (°C)	Reaction	Label	P (bar)	T (°C)	Reaction
CADWI152	32,400	574	3 Fe-Cld < Alm + 4 Dsp + H$_2$O	CS-a199	20,400	534	5Mg-Car < 3 Qtz + 4 Ky + Cln + 6 H$_2$O
CADWI153	33,400	620	3 Fe-Cld > Alm + 4 Dsp + H$_2$O	CS-a190	18,500	569	5Mg-Car > 3 Qtz + 4 Ky + Cln + 6 H$_2$O
CADWI154	32,400	529	3 Fe-Cld < Alm + 4 Dsp + H$_2$O	CS-a177	18,200	512	5Mg-Car > 3 Qtz + 4 Ky + Cln + 6 H$_2$O
CADWI157	32,400	571	3 Fe-Cld < Alm + 4 Dsp + H$_2$O	CS-a175	17,000	554	5Mg-Car > 3 Qtz + 4 Ky + Cln + 6 H$_2$O
CADWIT23	29,500	575	3 Fe-Cld < Alm + 4 Dsp + H$_2$O	CS-a150	14,500	513	5Mg-Car > 3 Qtz + 4 Ky + Cln + 6 H$_2$O
CADWIT26	29,500	585	3 Fe-Cld < Alm + 4 Dsp + H$_2$O	CS-a065	6,000	435	5Mg-Car > 3 Qtz + 4 Ky + Cln + 6 H$_2$O
CADWIT52	29,500	595	3 Fe-Cld < Alm + 4 Dsp + H$_2$O	CS-c190	19,500	530	14Mg-Car < 3Mg-Tlc + 13 Ky + Cln + 21 H$_2$O
CADWIT21	29,500	610	3 Fe-Cld < Alm + 4 Dsp + H$_2$O	CS-c191	18,600	562	14Mg-Car > 3Mg-Tlc + 13 Ky + Cln + 21 H$_2$O
CADWIT56	30,500	640	3 Fe-Cld > Alm + 4 Dsp + H$_2$O	CS-c300	30,500	564	14Mg-Car < 3Mg-Tlc + 13 Ky + Cln + 21 H$_2$O
CADWIT24	30,500	653	3 Fe-Cld > Alm + 2 Co + 3 H$_2$O	CS-c299	29,400	592	14Mg-Car > 3Mg-Tlc + 13 Ky + Cln + 21 H$_2$O
CADWIT58	30,500	655	3 Fe-Cld > Alm + 2 Co + 3 H$_2$O	CSd20543	20,500	537	3Mg-Car + Qtz < Mg-Tlc + 3 Ky + 5 H$_2$O
CADWIT57	30,500	655	3 Fe-Cld > Alm + 2 Co + 3 H$_2$O	CSd20561	19,500	566	3Mg-Car + Qtz > Mg-Tlc + 3 Ky + 5 H$_2$O
CADWIT50	27,500	575	3 Fe-Cld < Alm + 2 Co + 3 H$_2$O	CSd20560	30,600	555	3Mg-Car + Qtz < Mg-Tlc + 3 Ky + 5 H$_2$O
CADWIT54	27,500	615	3 Fe-Cld < Alm + 2 Co + 3 H$_2$O	CSd20580	29,600	585	3Mg-Car + Qtz > Mg-Tlc + 3 Ky + 5 H$_2$O
CADWIT31	26,500	585	3 Fe-Cld < Alm + 2 Co + 3 H$_2$O	CSd25000	25,500	548	3Mg-Car + Qtz < Mg-Tlc + 3 Ky + 5 H$_2$O
CADWIT32	25,500	575	3 Fe-Cld < Alm + 2 Co + 3 H$_2$O	CSd25001	24,500	572	3Mg-Car + Qtz > Mg-Tlc + 3 Ky + 5 H$_2$O
CADWIT47	25,500	585	3 Fe-Cld < Alm + 2 Co + 3 H$_2$O	CS-eaa1	9,600	400	5Mg-Car + 9 Qtz < 4 Prl + Cln + 2 H$_2$O
CADWIT33	25,500	610	3 Fe-Cld < Alm + 2 Co + 3 H$_2$O	CS-eaa2	7,600	400	5Mg-Car + 9 Qtz > 4 Prl + Cln + 2 H$_2$O
CADWIT37	24,500	640	3 Fe-Cld > Alm + 2 Co + 3 H$_2$O	CS-ebb1	9,460	350	5Mg-Car + 9 Qtz < 4 Prl + Cln + 2 H$_2$O
CADWIT38	24,500	647	3 Fe-Cld > Alm + 2 Co + 3 H$_2$O	CS-ebb2	7,460	350	5Mg-Car + 9 Qtz > 4 Prl + Cln + 2 H$_2$O
CADWIT34	24,500	660	3 Fe-Cld > Alm + 2 Co + 3 H$_2$O	CS-ecc1	9,300	300	5Mg-Car + 9 Qtz < 4 Prl + Cln + 2 H$_2$O
CADWIT35	24,500	680	3 Fe-Cld > Alm + 2 Co + 3 H$_2$O	CS-ecc2	6,300	300	5Mg-Car + 9 Qtz > 4 Prl + Cln + 2 H$_2$O
CADWIT57b	24,500	685	3 Fe-Cld > Alm + 2 Co + 3 H$_2$O	CS-22a	22,000	358	Fe-Car < Qtz + Fe-Cld + H$_2$O
CACWI-12	13,000	565	3 Fe-Cld < Alm + 2 Co + 3 H$_2$O	CS-22b	22,000	408	Fe-Car > Qtz + Fe-Cld + H$_2$O
CACWI-11	12,000	600	3 Fe-Cld > Alm + 2 Co + 3 H$_2$O	CS-19a	19,000	358	Fe-Car < Qtz + Fe-Cld + H$_2$O
CACWI-22	20,500	607	3 Fe-Cld < Alm + 2 Co + 3 H$_2$O	CS-19b	19,000	408	Fe-Car > Qtz + Fe-Cld + H$_2$O
CACWI-14	19,500	645	3 Fe-Cld > Alm + 2 Co + 3 H$_2$O	CS-15a	15,000	356	Fe-Car < Qtz + Fe-Cld + H$_2$O
CS-1828a	18,785	575	5Mg-Cld < 2 Co + 2 Ky + Cln + H$_2$O	CS-15b	15,000	406	Fe-Car > Qtz + Fe-Cld + H$_2$O
CS-1828b	17,785	575	5Mg-Cld > 2 Co + 2 Ky + Cln + H$_2$O	CS-115a	11,500	350	Fe-Car < Qtz + Fe-Cld + H$_2$O
CS-1921a	19,715	600	5Mg-Cld < 2 Co + 2 Ky + Cln + H$_2$O	CS-115b	11,500	400	Fe-Car > Qtz + Fe-Cld + H$_2$O
CS-1921b	18,715	600	5Mg-Cld > 2 Co + 2 Ky + Cln + H$_2$O	CS-09a	9,000	343	Fe-Car < Qtz + Fe-Cld + H$_2$O
CS-2034a	20,840	625	5Mg-Cld < 2 Co + 2 Ky + Cln + H$_2$O	CS-09b	9,000	393	Fe-Car > Qtz + Fe-Cld + H$_2$O
CS-2034b	19,840	625	5Mg-Cld > 2 Co + 2 Ky + Cln + H$_2$O	CS-07a	7,000	333	Fe-Car < Qtz + Fe-Cld + H$_2$O
CS-2157a	22,070	650	5Mg-Cld < 2 Co + 2 Ky + Cln + H$_2$O	CS-07b	7,000	383	Fe-Car > Qtz + Fe-Cld + H$_2$O
CS-2157b	21,070	650	5Mg-Cld > 2 Co + 2 Ky + Cln + H$_2$O				
CS-2315a	23,650	675	5Mg-Cld < 2 Co + 2 Ky + Cln + H$_2$O				
CS-2315b	22,650	675	5Mg-Cld > 2 Co + 2 Ky + Cln + H$_2$O				
CS-2330a	25,300	700	5Mg-Cld < 2 Co + 2 Ky + Cln + H$_2$O				
CS-2330b	24,300	700	5Mg-Cld > 2 Co + 2 Ky + Cln + H$_2$O				

For each reaction, assemblages on the left-hand side of the " < " sign are stable, and vice-versa. CACWI: Ganguly (1969); CADWIT and CADWI: Vidal etal. (1994); CS: Chopin and Schreyer (1983)

References

Abraham K, Schreyer W (1976) A talc-phengite assemblage in piemontite schist from Brezovica, Serbia, Yugoslavia. J Petrol 17:421–439

Bearth P (1952) Geologie und Petrographie des Monte Rosa. Beitr Geol Karte Schweiz. NF, vol 96, 94 pp

Berman RG (1988) Internally consistent thermodynamic data for minerals in the system Na_2O–K_2O–CaO–MgO–FeO–Fe_2O_3–Al_2O_3–SiO_2–TiO_2–H_2O –CO_2. J Petrol 29:445–522

Berman RG (1990) Mixing properties of Ca–Mg–Fe–Mn garnets. Am Mineral 75:328–344

Berman RG, Brown TH (1985) Heat capacity in the system Na_2O–K_2O–CaO–MgO–FeO–Fe_2O_3–Al_2O_3–SiO_2–TiO_2–H_2O–CO_2: representation, estimation, and high temperature extrapolation. Contrib Mineral Petrol 89:168–183

Biino GG, de Capitani C (1995) Equilibrium assemblage calculations: a new approach to metamorphic petrology. In: Lombardo B (ed) Studies on metamorphic rocks and minerals of the western Alps. A volume in memory of Ugo Pognante, vol 13. Bollettino Museo Regionale di Scienze Naturali, Torino, pp 11–53

de Capitani C (1994) Gleichgewichts-Phasendiagramme: Theorie und Software. Beih Eur J Mineral 6:48

de Capitani C, Brown TH (1987) The computation of chemical equilibrium in complex systems containing non-ideal solutions. Geochim Cosmochim Acta 51:2639–2652

Chinner GA, Dixon JE (1973) Some high-pressure parageneses of the Allalin gabbro, Valais, Switzerland. J Petrol 14:185–202

Chopin C (1979) De la Vanoise au massif du Grand Paradis: une approche pétrographique et radiochronologique de la signification géodynamique du métamorphisme de haute pression. Thèse 3ème cycle. Université Paris VI, 145 pp

Chopin C (1981) Talc–phengite: a widespread assemblage in high-grade pelitic blueschists of the Western Alps. J Petrol 22:628–650

Chopin C (1983) Magnesiochloritoid, a key-mineral for the petrogenesis of high-grade pelitic blueschists. Bull Mineral 106:715–717

Chopin C (1984) Coesite and pure pyrope in high-grade blueschists of the Western Alps: a first record and some consequences. Contrib Mineral Petrol 86:107–118

Chopin C, Monié P (1984) A unique magnesiochloritoid-bearing, high-pressure assemblage from the Monte Rosa, Western Alps: petrologic and $^{40}Ar/^{39}Ar$ radiometric study. Contrib Mineral Petrol 87:388–398

Chopin C, Schreyer W (1983) Magnesiocarpholite and magnesiochloritoid: two index minerals of pelitic blueschists and their preliminary phase relations in the model system MgO–Al_2O_3–SiO_2–H_2O. Am J Sci Orville 283-A:72–96

Chopin C, Henry C, Michard A (1991) Geology and petrology of the coesite-bearing terrain, Dora Maira massif, Western Alps. Eur J Mineral 3:263–291

Comodi P, Mellini M, Zanazzi PF (1992) Magnesiochloritoid: compressibility and high-pressure structure refinement. Phys Chem Miner 18:483–490

Dal Piaz GV (1971) Nuovi ritrovamenti di cianite alpina nel cristallino antico del Monte Rosa. Rend Soc Ital Miner Petrol 27:437–477

Dal Piaz GV, Lombardo B (1986) Early Alpine eclogite metamorphism in the Penninic Monte Rosa-Gran Paradiso basement nappes of the northwestern Alps. In: Evans BW, Brown EH (eds) Blueschists and eclogites, mem 164. Geological Society of America, Boulder, pp 249–265

Demény A, Sharp Z, Pfeifer HR (1997) Mg–metasomatism and formation conditions of Mg–chlorite–muscovite–quartzphyllites (leucophyllites) of Eastern Alps (W Hungary) and their relations to alpine whiteschists. Contrib Mineral Petrol 128:247–260

El-Shazly AK, Liou JG (1991) Glaucophane chloritoid bearing assemblages from NE Oman; Petrologic significance and a petrogenetic grid for high P/T metapelites. Contrib Mineral Petrol 107:180–201

Escher A, Masson H, Steck A (1993) Nappe geometry in the Western Swiss Alps. J Struct Geol 15:501–509

Ganguly J (1969) Chloritoid stability and related parageneses: theory, experiments and applications. Am J Sci 267:910–944

Hetherington CJ, Le Bayon R (2005) Bulk rock composition: a key to identifying invisible prograde reactions in zoned garnet. Schweiz Mineral Petrogr Mitt 85 (in press)

Holland TJB, Powell R (1990) An enlarged and updated internally consistent thermodynamic dataset with uncertainties and correlations: the system K_2O–Na_2O–CaO–MgO–FeO–Fe_2O_3–Al_2O_3–TiO_2–SiO_2–C–H_2O–O_2. J Metamorph Geol 8:89–124

Holland TJB, Baker J, Powell R (1998) Mixing properties and activity–composition relationships of chlorites in the system MgO–FeO–Al_2O_3–SiO_2–H_2O. Eur J Mineral 10:395–406

Ivaldi G, Catti M, Ferraris G (1988) Crystal structure at 25°C and 700°C of magnesiochloritoid from a high-pressure assemblage (Monte Rosa). Am Mineral 73:358–364

Kretz R (1983) Symbols for rock-forming minerals. Am Mineral 68:277–279

Laird J (1988) Chlorites: metamorphic petrology. In: Bailey SW (ed) Hydrous phyllosilicates (exclusive of micas), reviews in mineralogy, vol 19. Mineralogical Society of America, pp 405–453

Loomis TP (1983) Compositional zoning of crystals: a record of growth and reaction history. In: Saxena SK (ed) Kinetics and equilibrium in mineral reactions. Springer, Berlin Heidelberg New York, pp 1–60

Massonne H-J (1992) Evidence for low-temperature ultrapotassic siliceous fluids in subduction zone environments from experiments in the system K_2O–MgO–Al_2O_3–SiO_2–H_2O (KMASH). Lithos 28:421–434

Massonne H-J, Schreyer W (1989) Stability field of the high-pressure assemblage talc + phengite and two new phengite barometers. Eur J Mineral 1:391–410

Massonne HJ, Szpurka Z (1997) Thermodynamic properties of white micas on the basis of high-pressure experiments in the systems K_2O–MgO–Al_2O_3–SiO_2–H_2O and K_2O–FeO–Al_2O_3–SiO_2–H_2O. Lithos 41:229–250

Miller C (1986) Alpine high-pressure metamorphism in the Eastern Alps. Schweiz Mineral Petrogr Mitt 66:139–144

Murtagh BA, Saunders MA (1987) Minos 5.1 user's guide. Technical Report SOL 83–20 R. Systems Optimization Laboratory, Stanford University

Nagel T, de Capitani C, Frey M (2002) Isograds and P–T evolution in the eastern Lepontine Alps (Graubünden, Switzerland). J Metamorph Geol 20:309–324

Pawlig S, Baumgartner LP (2001) Geochemistry of a talc-kyanite-chloritoid shear zone within the Monte Rosa granite, Val d'Ayas, Italy. Schweiz Mineral Petrogr Mitt 81:329–346

Schertl H-P, Schreyer W, Chopin C (1991) The pyrope-coesite rocks and their country rocks at Parigi, Dora Maira massif, western Alps: detailed petrography, mineral chemistry and PT-path. Contrib Mineral Petrol 108:1–21

Schmid SM, Kissling E (2000) The arc of the western Alps in the light of geophysical data on deep crustal structure. Tectonics 19:62–85

Schreyer W (1973) Whiteschists: a high-pressure rock and its geological significance. J Geol 81:735–739

Schreyer W (1974) Whiteschists, a new type of metamorphic rock formed at high-pressures. Geol Rund 43:127–144

Schreyer W (1977) Whiteschists: their composition and pressure-temperature regimes based on experimental, field, and petrographic evidence. Tectonophysics 43:127–144

Schreyer W (1988) Experimental studies on metamorphism of crustal rocks under mantle pressures. Mineral Mag 52:1–26

Schreyer W, Seifert F (1969) Compatibility relations of the aluminium silicates in the systems MgO–Al_2O_3–SiO_2–H_2O and K_2O–MgO–Al_2O_3–SiO_2–H_2O at high-pressures. Am J Sci 267:371–388

Schreyer W, Massonne H-J, Chopin C (1987) Continental crust subducted to mantle depths near 100 km: Implications for magma and fluid genesis in collision zones. In: Mysen BO (ed) Magmatic processes: physico-chemical principles, vol 1. Special Publication of the Geochemical Society, pp 155–163

Sharp ZD, Essene EJ, Hunzicker JC (1993) Stable isotope geochemistry and phase equilibria of coesite-bearing whiteschists, Dora-Maira Massif, western Alps. Contrib Mineral Petrol 114:1–12

Spear FS (1988) Metamorphic fractional crystallization and internal metasomatism by diffusional homogenization of zoned garnets. Contrib Mineral Petrol 99:507–517

Spear FS, Cheney JT (1989) A petrogenetic grid for pelitic schists in the system SiO_2–Al_2O_3–FeO–MgO–K_2O–H_2O. Contrib Mineral Petrol 101:149–164

Spicher A (1980) Tektonische Karte der Schweiz, scale 1:500 000, 2nd edn. Schweizerische Geologische Komission, Bern

Thompson JB Jr (1957) The graphical analysis of mineral assemblages in pelitic schists. Am Mineral 42:842–858

Tilton GR, Schreyer W, Schertl H-P (1991) Pb–Sr–Nd isotopic behavior of deeply subducted crustal rocks from the Dora-Maira Massif, Western Alps, Italy-II: what is the age of ultrahigh-pressure metamorphism?. Contrib Mineral Petrol 108:22–33

Todd CS, Engi M (1997) Metamorphic field gradients in the central Alps. J Metamorph Geol 15:513–530

Vearncombe JR (1983) High pressure–low temperature metamorphism in the Gran Paradiso basement, western Alps. J Metamorph Geol 1:103–115

Vidal O, Goffé B, Theye Th (1992) Experimental study of the stability of sudoite and magnesiocarpholite and calculation of a new petrogenetic grid for the system FeO–MgO–Al_2O_3–SiO_2–H_2O. J Metamorph Geol 10:603–614

Vidal O, Theye Th, Chopin C (1994) Experimental study of chloritoid stability at high pressure and various fO_2 conditions. Contrib Mineral Petrol 118:256–270

Vidal O, Parra T, Trotet F (2001) A thermodynamic model for Fe–Mg aluminous chlorite using data from phase equilibrium experiments and natural pelitic assemblages in the 100–600°C, 1–25 kb range. Am J Sci 301:557–592

Vrana S, Barr MWC (1972) Talc-kyanite-quartz schists and other high-pressure assemblages from Zambia. Mineral Mag 38:837–846